Cell

Generation and Dynamics of an Endogenous, Self-Generated Signaling Gradient across a Migrating Tissue

Gayatri Venkiteswaran,[1,5] Stephen W. Lewellis,[1,5] John Wang,[1] Eric Reynolds,[1,2] Charles Nicholson,[3] and Holger Knaut[1,4,*]

[1]Developmental Genetics Program, Skirball Institute of Biomolecular Medicine, New York University Langone Medical Center, New York, NY 10016, USA

[2]Charite Universitätsmedizin Berlin, 10117 Berlin, Germany

[3]Department of Neuroscience and Physiology, New York University Langone Medical Center, New York, NY 10016, USA

[4]Kimmel Center for Stem Cell Biology, New York University Langone Medical Center, New York, NY 10016, USA

[5]These authors contributed equally to this work

*Correspondence: holger.knaut@med.nyu.edu

http://dx.doi.org/10.1016/j.cell.2013.09.046

SUMMARY

In animals, many cells reach their destinations by migrating toward higher concentrations of an attractant. However, the nature, generation, and interpretation of attractant gradients are poorly understood. Using a GFP fusion and a signaling sensor, we analyzed the distribution of the attractant chemokine Sdf1 during migration of the zebrafish posterior lateral line primordium, a cohort of about 200 cells that migrates over a stripe of cells uniformly expressing *sdf1*. We find that a small fraction of the total Sdf1 pool is available to signal and induces a linear Sdf1-signaling gradient across the primordium. This signaling gradient is initiated at the rear of the primordium, equilibrates across the primordium within 200 min, and operates near steady state. The rear of the primordium generates this gradient through continuous sequestration of Sdf1 protein by the alternate Sdf1-receptor Cxcr7. Modeling shows that this is a physically plausible scenario.

INTRODUCTION

During animal development, homeostasis, and disease, cells must move from one location to another to form tissues, assemble into organs, chase a pathogen or—in the case of cancer—populate sites of metastasis. Depending on the process, cells migrate as single cells, as chains of cells, or as tissue-like collectives of a few cells to hundreds of cells. In order to move in the correct direction, migrating cells need guidance cues. Studies over the last few decades have revealed the identity of many guidance cues. These guidance cues are often secreted from the target tissue and form an attractant gradient, from which migrating cells derive directional information (Parent and Devreotes, 1999; Rørth, 2011; Swaney et al., 2010). There are several ways that these attractant gradients can guide migrating cells. For example, migrating cells can be guided by long-range attractant gradients emanating from a source at the target tissue (Montell, 2003), shifting expression domains of the attractant (Affolter and Caussinus, 2008) or the graded distribution of an immobilized attractant (Weber et al., 2013). In the simplest model, attractants are secreted from a local source and degraded by a local sink, generating a linear gradient at steady state. Francis Crick showed in 1970 that this source-sink model can generate stable, linear gradients over several hundreds of micrometers (Crick, 1970).

A classic example for single-cell migration is the slime mold Dictyostelium (reviewed in Parent and Devreotes, 1999). Dictyostelium cells are attracted by cAMP and move toward higher cAMP concentrations. The cells are about 10 μm in diameter, and though they can sense differences in cAMP concentration of as low as 1% across themselves, they migrate most efficiently when this difference is 3% (Fisher et al., 1989). Intriguingly, Dictyostelium migrate toward higher cAMP concentrations both within pre-steady-state gradients with temporally increasing cAMP concentration and within stable, steady-state gradients (Fisher et al., 1989). It is thought that Dictyostelium achieves sensitivity to concentration differences of cAMP and robustness to fluctuations in cAMP concentration by integrating and reinforcing information about local cAMP concentrations sensed by the cAMP receptors on the cell surface (Cai and Devreotes, 2011).

The purpose of this study is to determine the shape (linear or nonlinear), dynamics (pre-steady-state or steady-state), and mechanisms of generation and maintenance of an attractant gradient in a living animal. We were motivated by recent studies using overexpressed fluorescently tagged proteins to describe the distribution of signaling molecules in living animals (Entchev et al., 2000; Kicheva et al., 2007; Müller et al., 2012; Teleman and Cohen, 2000; Yu et al., 2009). These studies reported the distribution of the total population of signaling molecules using overexpressed tagged molecules, but they did not delineate how much of the total signaling molecules are actually involved in

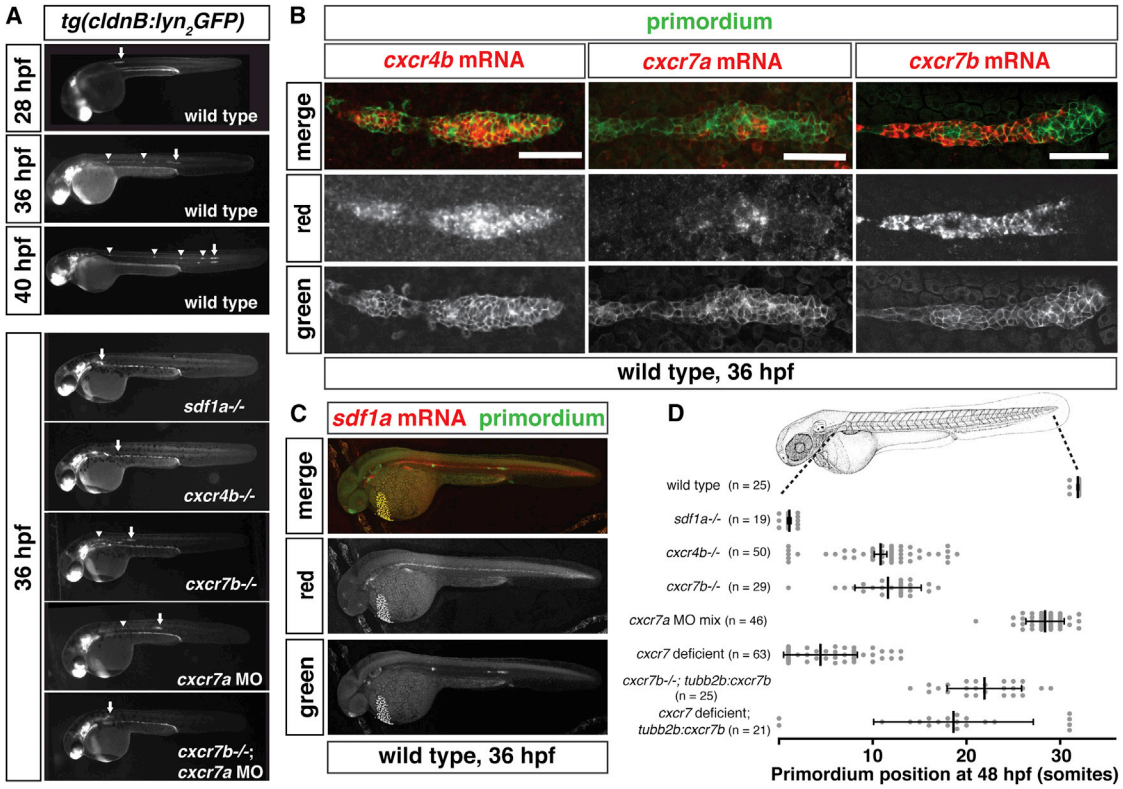

Figure 1. Expression and Requirement of Sdf1a and Its Receptors Cxcr4b, Cxcr7a, and Cxcr7b during Primordium Migration

(A) Live images of embryos of the indicated stage and genotype. Arrow indicates the primordium, and arrowheads indicate neuromasts.

(B) Fluorescent staining for *cxcr4b*, *cxcr7a*, or *cxcr7b* mRNA and GFP protein at 36 hpf. Scale bar, 50 μm.

(C) Fluorescent staining for *sdf1a* mRNA and GFP protein in a *tg(cldnB:lyn$_2$GFP)* embryo at 36 hpf. Anterior is to the left, and posterior is to the right.

(D) Quantification of primordium migration in 48 hpf embryos of indicated genotypes. The vertical bars represent the average position of the primordium, the error bars represent SD, and the circles represent the positions of individual primordia. 48 hpf embryo schematic adapted from (Kimmel et al., 1995).

See also Figure S6.

signaling events. Therefore, the in vivo distribution of endogenous untagged signaling molecules remains unclear.

The posterior lateral line primordium in zebrafish is an excellent model for studying how attractants guide migrating cells (Aman and Piotrowski, 2010). The primordium is composed of about 200 epithelial-like cells that are born behind the ear around 19 hr postfertilization (hpf). During the next 20 hr, these cells migrate collectively along the body of the fish until they reach the tip of the tail around 40 hpf (Figure 1A and Movie S1 available online). During this migration period, the primordium deposits five to seven cell clusters along the trunk and tail of the embryo (Ghysen and Dambly-Chaudière, 2007). Each of these clusters differentiates into a neuromast, a specialized organ that senses water flow around the embryo. The primordium requires the chemokine Sdf1a and its two receptors, Cxcr4b and Cxcr7b, for proper migration (Figure 1A). The cells of the primordium express *cxcr4b* uniformly starting at 19 hpf when the primordium first forms (Figure 1B). *cxcr7b* expression turns on specifically in the rear of the primordium (Figure 1B) only once it reaches and starts migrating over a narrow and uniform stripe of *sdf1a*-expressing cells located along the trunk and tail of the embryo (Figure 1C) (Breau et al., 2012; Dambly-Chaudière et al., 2007; David et al., 2002; Valentin et al., 2007). Although chemokine signaling is required for proper migration, it remains unclear how a stripe of uniform *sdf1a* can provide directional guidance to the primordium during its journey through the embryo.

Here, we developed quantitative reporters for Sdf1a protein and Sdf1 signaling and employed quantitative imaging and mathematical modeling to examine the distribution of total Sdf1a protein and the pool of Sdf1a protein available for signaling through Cxcr4. We find that total Sdf1a protein is distributed uniformly along the stripe of chemokine-producing cells underneath the primordium. In contrast, Sdf1 signaling is linearly graded across the primordium for the duration of its migration, with a slope of 7% per cell. Upon abrogation, this gradient re-emerges and reaches steady state again within 200 min. Mathematical modeling shows that the observed gradient kinetics are inconsistent with freely diffusing Sdf1a protein and suggest that the chemokine is hindered in its diffusivity, probably due to binding to extracellular molecules.

To determine how the primordium converts a uniform source of Sdf1a protein into an Sdf1-signaling gradient, we analyzed the expression of Sdf1a protein within the primordium. We find that the rear of the primordium sequesters 1% of the total

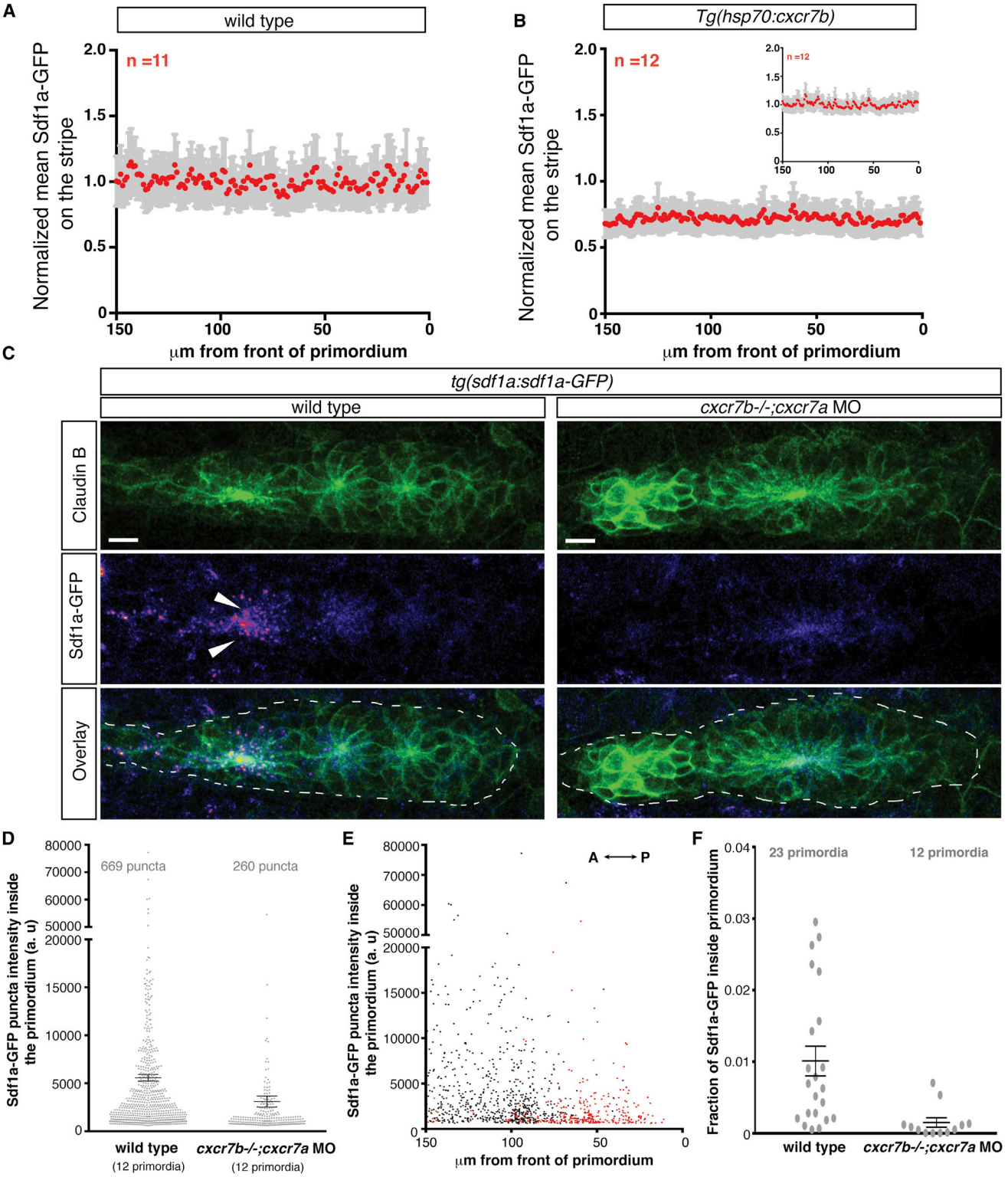

Figure 2. Cxcr7 Is Required for Sdf1a-GFP Sequestration by the Primordium

(A and B) Average fluorescence intensity of Sdf1a-GFP protein along the stripe of chemokine-producing cells underneath primordia in embryos of indicated genotypes (B, inset, heat-shocked wild-type control embryos).

(C) Sum projection of the primordium from 36 hpf embryos of indicated genotypes stained for Claudin-B and GFP. Scale bar, 10 μm. Direction of migration is to the right. Arrowheads indicate Sdf1a-GFP puncta.

(legend continued on next page)

Sdf1a protein. Although controversial (Rajagopal et al., 2009), CXCR7—an alternate receptor for SDF1—has been proposed to act as a chemokine clearance receptor (Boldajipour et al., 2008; Sánchez-Alcañiz et al., 2011). The two CXCR7 orthologs, Cxcr7a and Cxcr7b, are expressed in the rear of the primordium. We find that the two orthologs are required for Sdf1a protein uptake in the rear of the primordium, Sdf1-signaling gradient formation across the primordium, and primordium migration. Additionally, in embryos lacking Cxcr7, both the Sdf1-signaling gradient and primordium migration can be restored by reintroducing Cxcr7b underneath the rear of the primordium. These observations demonstrate that the primordium generates an attractant gradient across itself by sequestering Sdf1a protein in its rear via Cxcr7-mediated chemokine uptake. This self-generated attractant gradient, combined with the route information provided by the stripe of *sdf1a*-expressing cells, then provides directional guidance to the migrating primordium. Mathematical modeling of a sink moving across a source stripe that provides a constant attractant concentration shows that this is a plausible scenario.

RESULTS

Sdf1a-GFP Is Distributed Evenly along the Migratory Route of the Primordium

To analyze the distribution of Sdf1a protein along the migratory route of the primordium, we generated a transgenic line (*tg(sdf1a:sdf1a-GFP)*) that expresses Sdf1a fused to green fluorescent protein (GFP) from a bacterial artificial chromosome (BAC). This BAC includes the *sdf1a* exons and introns, a 55 kb sequence upstream of the start codon, and a 30 kb sequence downstream of the stop codon (Figure S1A). The transgene recapitulates the endogenous *sdf1a* mRNA expression pattern (Figures S1B and S1C) and restores primordium migration in *sdf1a* mutant embryos (Figures S1E–S1G), demonstrating that it is functional. We used the *tg(sdf1a:sdf1a-GFP)* line to examine the distribution of Sdf1a-GFP protein in wild-type embryos. Sdf1a-GFP protein is distributed evenly along the migration route of the primordium (Figure S1D) and is confined to the immediate vicinity of the cells that produce it (Movie S2). We quantified the intensity of Sdf1a-GFP on the stripe underneath the primordium and do not detect a difference in the levels of the chemokine between the front and rear of the primordium (Figure 2A and Data S1). However, close inspection reveals that cells in the rear of the primordium sequester small amounts of Sdf1a-GFP, which appear as discrete intracellular puncta (Figure 2C and Movie S2). Quantification of the number and intensity of Sdf1a-GFP puncta inside the primordia of multiple embryos confirms that cells in the rear of the primordium internalize more Sdf1a-GFP than the cells in the front of the primordium (Figure 2E and Data S2). This raises the possibility that the rear of the primordium reduces the concentration of Sdf1a beneath it through protein sequestration, suggesting that the primordium is capable of locally modifying the levels of chemokine in its path. However, the Sdf1a-GFP uptake by the rear of the primordium represents only 1% of the total Sdf1a-GFP signal (Figure 2F) and is thus within the noise margin (SEM 18%) of Sdf1a-GFP intensity measurements made from the stripe beneath the primordium. This suggests that the migrating primordium only modifies the chemokine pool in its immediate vicinity, with minimal effects on overall chemokine levels.

A Novel In Vivo Sdf1-Signaling Sensor

It is possible that the primordium senses and responds to a shallow gradient of Sdf1a that we cannot detect by measuring the total amount of Sdf1a-GFP protein along the stripe. To investigate this possibility, we developed an in vivo Sdf1-signaling sensor designed to measure the levels of Sdf1a that the primordium perceives. Because the binding of SDF1 to CXCR4 triggers rapid internalization of the receptor from the cell membrane and subsequent receptor degradation (Marchese and Benovic, 2001; Marchese et al., 2003; Minina et al., 2007), we reasoned that the levels of Cxcr4b on the cell membrane should correlate inversely to the levels of extracellular Sdf1 protein. To test this idea, we fused the monomeric red fluorescent protein Kate2 to the C terminus of Cxcr4b (Cxcr4b-Kate2) and expressed this fusion protein from the *cxcr4b* promoter. As an internal reference, we coexpressed membrane-tethered GFP (memGFP) that is co-translated from the same transcript through an internal ribosomal entry site (IRES) (Figures 3A and S1H). This signaling sensor recapitulates the expression of endogenous *cxcr4b* (Figures S1I–S1K), internalizes with Sdf1a-GFP (Figures S1O and S1P), and rescues primordium migration in *cxcr4b* mutant embryos (Figure S1L–S1N), demonstrating that it is functional. Because ligand binding causes receptor internalization, the ratio of red fluorescence from the Cxcr4b-Kate2 fusion protein to green fluorescence from the memGFP on the membrane of a cell (FmemRed/FmemGreen) should represent a quantitative readout of the amount of Sdf1a protein to which the cell is exposed (Figure 3B). We tested the relationship between Sdf1a protein levels and the Sdf1-signaling sensor in several ways. First, in the absence of Sdf1a protein, the membranes of cells within the primordium exhibit high levels of Cxcr4b-Kate2, resulting in an average FmemRed/FmemGreen ratio of 2.6 (Figures 3H and 3I, column 4, and Data S3). Second, upon global Sdf1a overexpression from an inducible heat shock promoter (*tg(hsp70:sdf1a)*), Cxcr4b-Kate2 is found primarily inside of the cell rather than on the cell membrane, resulting in an average FmemRed/FmemGreen ratio of 0.2 (Figures 3H and 3I, column 5). Third, injection of increasing amounts of a translation-blocking *sdf1a* morpholino progressively shifts the FmemRed/FmemGreen ratios across the primordium to higher

(D) Distribution of intensities of Sdf1a-GFP puncta in primordia of indicated genotypes.
(E) Distribution of intensities of Sdf1a-GFP puncta in primordia along the anterior-posterior axis. Each dot (D and E) represents an individual punctum (red, *cxcr7b*$^{-/-}$*; cxcr7a* morphant primordia; black, wild-type primordia).
(F) Fraction of Sdf1a-GFP found inside of the primordium of the total Sdf1a-GFP in the indicated genotype. Each dot represents the fraction of Sdf1a-GFP in an individual primordium. Horizontal bars represent the mean ± SEM.
See also Figure S1 and Data S1 and S2.

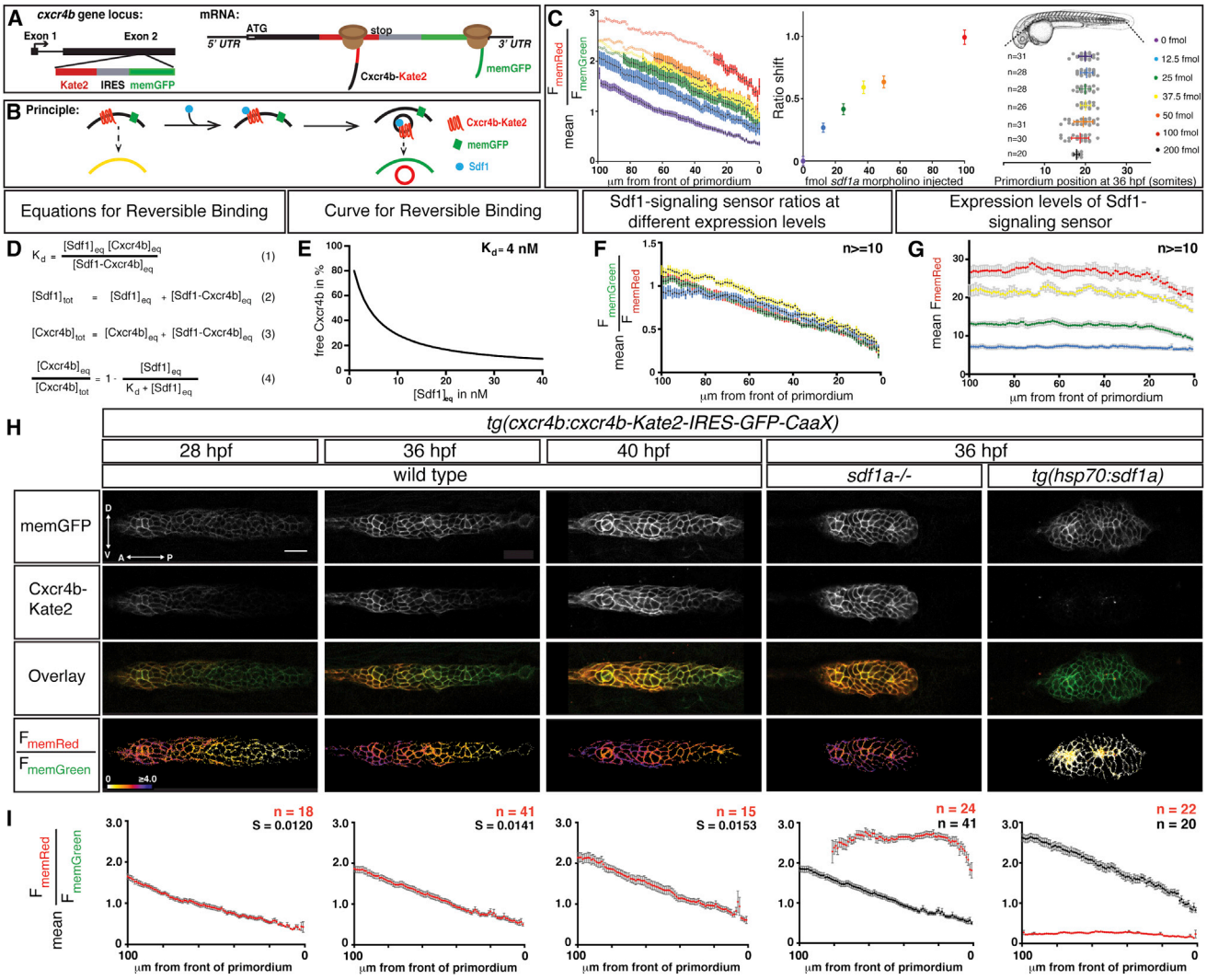

Figure 3. A Quantitative Signaling Reporter for Sdf1

(A and B) Schematic of Sdf1-signaling sensor construct (A) and concept (B).

(C) (Left) Mean FmemRed/FmemGreen ratio along the anterior-posterior axis of n ≥ 20 primordia from *tg(cxcr4b:cxcr4b-Kate2-IRES-GFP-CaaX)* embryos injected with *sdf1a* morpholino. Circles are mean ratios, and error bars represent SEM. Open circles indicate ratios greater than the SD corrected mean FmemRed/FmemGreen ratio in *sdf1a*$^{-/-}$ primordia. (Middle) Shift of the FmemRed/FmemGreen ratio curves on left. The error bars represent SD. (Right) Primordium position in embryos injected with increasing amounts of *sdf1a* morpholino. The vertical bars represent the average position of the primordium, the error bars represent SD, and the circles represent the positions of individual primordia. 35 hpf embryo schematic adapted from Kimmel et al., (1995).

(D) Derivation of equation for reversible binding of Sdf1 to Cxcr4b (Equation 4) using the definition of the dissociation constant (Equation 1) for the reversible reaction $Cxcr4b_{eq}+Sdf1_{eq} \rightleftharpoons Cxcr4b\text{-}Sdf1_{eq}$ (wherein $Cxcr4b_{eq}$ is free receptor, $Sdf1_{eq}$ is free ligand, and $Cxcr4b\text{-}Sdf1_{eq}$ is receptor-ligand complex) and mass balance for Sdf1 (Equation 2) and Cxcr4b (Equation 3).

(E) Graph of Equation 4 for a Kd of 4 nM (Crump et al., 1997).

(F) Mean FmemGreen/FmemRed ratio values across 100 µm beginning at the front of the primordium in 36 hpf wild-type embryos with increasing levels of expression of the signaling sensor indicated in (G).

(G) Mean FmemRed intensity values across 100 µm beginning at the front of the primordium in 36 hpf embryos carrying different combinations and copy numbers of the signaling sensor transgenes (blue, *Sdf1 sensorGRp1*/+, n = 14; green, *Sdf1 sensorGRp7*/+, n = 17; yellow, *Sdf1 sensorGRp1*/ *Sdf1 sensorGRp7*, n = 10; red, *Sdf1 sensorGRp7*/ *Sdf1 sensorGRp7*, n = 16). The colored and gray bars indicate SEM in (F) and (G), respectively.

(H) Single confocal slices through the primordium in live embryos of the indicated genotypes and stages, all carrying the Sdf1-signaling sensor. The FmemRed/FmemGreen images are inverted heat maps of the ratio.

(I) Mean FmemRed/FmemGreen along the anterior-posterior axis of n ≥ 10 primordia with 0 µm representing the front of each primordium. Red circles indicate the mean FmemRed/FmemGreen in embryos of the indicated genotype; black circles, where present, indicate the mean FmemRed/FmemGreen of wild-type embryos or heat-shocked control embryos. Gray bars indicate SEM. Anterior is to the left in (H). Scale bar, 20 µm.

See also Figures S1–S5 and Data S3, S4, and S5.

values in a manner that is directly proportional to the amount of *sdf1a* morpholino injected, consistent with progressively decreasing levels of Sdf1a (Figure 3C). Fourth, consistent with theoretical considerations for reversible ligand-receptor binding (Figures 3D and 3E), we find that altering the expression levels of the Sdf1-signaling sensor does not change the Sdf1-signaling sensor ratios across the primordium (Figures 3F and 3G). Fifth, in the absence of Sdf1a, Cxcr4b-Kate2 and memGFP are translated at a fairly constant ratio across the primordium (Figures 3H, column 4, and S2F), indicating that memGFP expression from the IRES is uniform across the primordium. Sixth, memGFP is expressed uniformly along the anterior-posterior axis of the primordium (Figure S2A and Data S5), indicating that the activity of the *cxcr4b* promoter is fairly constant across the cells of the primordium. Seventh, expression of the Sdf1-signaling sensor in HEK293T cells indicates that the FmemRed/FmemGreen ratios are directly proportional to the concentration of Sdf1 added to the culture media (Figures S3A and S3C). Thus, the ratio of FmemRed/FmemGreen reported by the Sdf1-signaling sensor is linearly related to the levels of Sdf1 protein that the primordium perceives during migration.

A Linear Sdf1-Signaling Gradient across the Primordium

Using this sensor, we detected an Sdf1-signaling gradient across the anterior-posterior axis of the migrating primordium in live, 36 hpf wild-type embryos (Figures 3H and 3I, column 2). The gradient begins at the leading edge of the primordium at a mean FmemRed/FmemGreen of below 0.6, increases fairly linearly by 1.2%/μm for the first 100 μm, and plateaus at a mean FmemRed/FmemGreen of 2.3 in the rear of the primordium (Figures 1, column 2, and S2G). The linear gradient moves with the primordium throughout its migration, remaining remarkably constant in shape and amplitude over time (Figures 3H and 3I, columns 1–3, and Movie S3, left). Moreover, the gradient is absent in *sdf1a* mutant embryos (Figure 3I, column 4) and is rapidly abolished upon global overexpression of Sdf1a from a heat-shock-inducible promoter (Figure 3I, column 5, and Movie S3, right), confirming that the signaling gradient depends on Sdf1a protein levels. The Sdf1-signaling gradient is mirrored by an internal gradient of internalized and degraded Cxcr4b. Quantification of the levels of internalized Cxcr4b-Kate2 to memGFP indicates that Cxcr4b-Kate2 is degraded more in the front than in the rear of the primordium and that internalization and degradation of Cxcr4b-Kate2 depends on Sdf1a (Figure S4 and Data S4). To approximate the lower and upper limits of Sdf1 signaling in the primordium, we compared the mean FmemRed/FmemGreen in *sdf1a* mutant embryos and embryos that globally overexpress Sdf1a. The maximal difference in chemokine signaling observed between these two scenarios is 2.4 ratio units (mean FmemRed/FmemGreen of 2.6 and 0.2, respectively, in Figure 3I, columns 4 and 5). When compared to the maximal signaling difference between the front and back of wild-type primordia of 1.7 ratio units (mean FmemRed/FmemGreen of 0.6 and 2.3, respectively, in Figure S1Q), this indicates that 36 hpf wild-type primordia use 71% of the Sdf1 signaling dynamic range.

The Sdf1-signaling gradient observed across the primordium—high signaling in the leading cells and low signaling in the trailing cells—suggests that a graded distribution of Sdf1a continuously confers directional information to the migrating primordium. Results from a previous study demonstrated that ectopic sources of the chemokine Sdf1b, the protein encoded by a closely related paralog of *sdf1a*, can attract the primordium (Li et al., 2004). Because Sdf1b is not expressed along the migratory route of the primordium and Sdf1b is dispensable for its migration, we hypothesized that Sdf1a, like Sdf1b, can lure the primordium off course when expressed ectopically, therefore acting as an instructive rather than permissive guidance cue. We tested this hypothesis in two ways. First, we overexpressed Sdf1a from a heat shock promoter during primordium migration in embryos carrying the *cldnB:lyn$_2$GFP* transgene or the Sdf1-signaling sensor. In response to global overexpression of Sdf1a, the primordium exhibits uniformly high levels of Cxcr4b-Kate2 internalization, rounds up, and ceases to migrate, in contrast to primordia in heat-shocked control embryos that report a steady, linear signaling gradient, maintain an elongated morphology, and continue to migrate (Figure S5A–S5C and Movie S3). Second, we generated small, Sdf1a-misexpressing clones along the migratory route of the primordium or within the primordium in *tg(cldnB:lyn$_2$GFP)* embryos by blastomere transplantation (Figure S5D). Clones positioned dorsal or ventral to the normal migratory route were able to attract the primordium, sending it off course (Figures S5J–S5L), whereas clones within the primordium caused it to round up and stall (Figure S5F).

Cxcr7 Sequesters Sdf1a Protein in the Rear of the Primordium

Our observations that the rear of the primordium sequesters Sdf1a-GFP protein (Figure 2C and Movie S2) and perceives lower levels of Sdf1 than the front (Figures 3H and 3I, columns 1–3) suggest that the rear of the primordium continuously clears Sdf1a protein from the region underneath itself. Previous studies have proposed that the alternate SDF1 receptor CXCR7 can act as a scavenger receptor for chemokines (Boldajipour et al., 2008; Sánchez-Alcañiz et al., 2011). Consistent with this proposition, *cxcr7b* is expressed in the rear of the primordium (Figure 1B, column 3) and is required for its migration (Figures 1A and 1D) (Dambly-Chaudière et al., 2007; Valentin et al., 2007). Primordia in *cxcr7b* mutant embryos exhibit slowed migration or stalling (Movie S4, top) (Valentin et al., 2007). Interestingly, we find that *cxcr7a*—the second ortholog of CXCR7 in zebrafish—is also expressed in the rear of the primordium (Figure 1B, column 2). In embryos injected with morpholinos that block translation of *cxcr7a* transcripts (Figures S6A and S6B), the primordium does not always reach the tip of the tail (Figures 1A and 1D). Compromising the function of both CXCR7 orthologs enhances these migration defects (Figures 1A and 1D), often resulting in complete stalling of the primordium (Movie S4, bottom), a defect that is comparable to what we observe in primordia of *sdf1a* mutant embryos (Figure 1A and Movie S1). However, in contrast to the rounded morphology that the primordium assumes in *sdf1a* mutant embryos (Figure 1A and Movie S1), primordia deficient in *cxcr7a* and *cxcr7b* (collectively referred to as Cxcr7) are more motile and often extend in multiple directions (Movie S4, bottom). Thus, Sdf1a protein sequestration by Cxcr7 is a plausible mechanism for the generation and maintenance of a

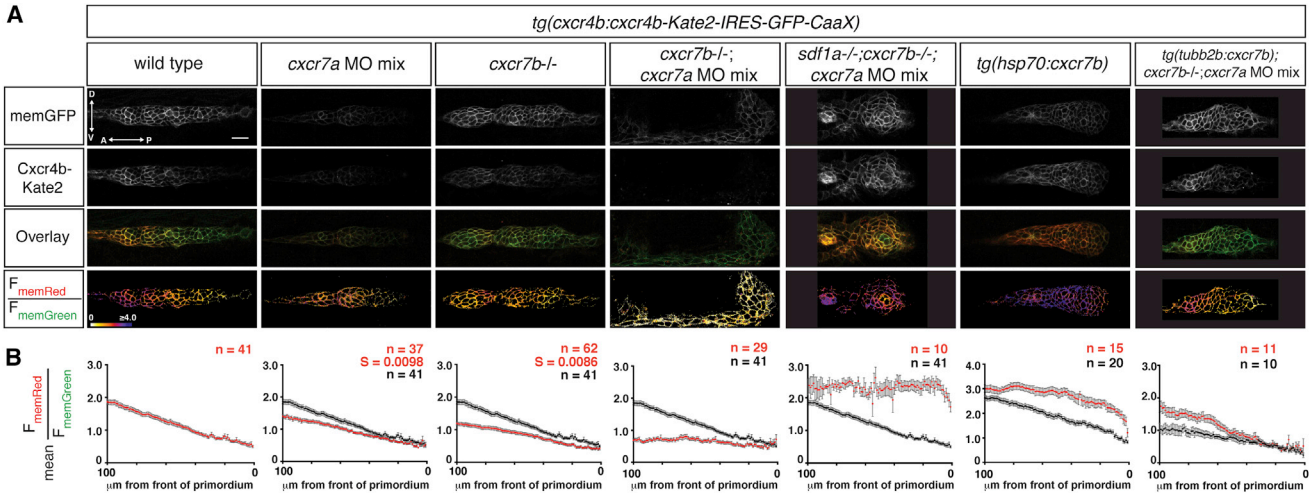

Figure 4. Cxcr7 Generates the Sdf1-Signaling Gradient across the Primordium

(A) Single confocal slices through the primordium in live 36 hpf embryos of the indicated genotypes, all carrying the Sdf1-signaling sensor. The FmemRed/FmemGreen images are inverted heat maps of the ratio.

(B) Mean FmemRed/FmemGreen along the anterior-posterior axis of n ≥ 10 primordia with 0 μm representing the front of each primordium. Red circles indicate the mean FmemRed/FmemGreen in embryos of the indicated genotype; black circles, where present, indicate the mean FmemRed/FmemGreen of wild-type embryos, heat-shocked control embryos, or *cxcr7*-deficient control embryos. Gray bars indicate SEM. Anterior is to the left, and dorsal is up in (A). Scale bar, 20 μm. Note that *cxcr7*-deficient*; tg(tubb2b:cxcr7b)* embryos were injected with a low dose of *cxcr7a* MO mix.

See also Figures S2, S4, and S6 and Extended Experimental Procedures.

chemokine attractant gradient across the migrating primordium. To test this, we measured Sdf1a-GFP protein uptake by the primordium in *cxcr7*-deficient and *cxcr7b*-overexpressing embryos. Consistent with the hypothesis, we find that *cxcr7*-deficient primordia fail to sequester Sdf1a-GFP protein in the rear of the primordium, in contrast to wild-type primordia that show significant uptake in this region (Figures 2C–2F and Movie S2). The number and intensity of the Sdf1a-GFP puncta are markedly reduced in *cxcr7* deficient primordia (Figures 2D and 2E), suggesting that Cxcr7 is required for chemokine sequestration. Conversely, overexpression of Cxcr7b from a heat-shock-inducible promoter causes the primordium to assume a rounded morphology similar to that observed in *sdf1a* mutant embryos and to decelerate (Movies S5 and S1, respectively). Sdf1a-GFP protein levels on the stripe outside of the primordium are reduced by 29% in these embryos (Figure 2B), indicating that Cxcr7 activity promotes removal of Sdf1a from the stripe.

Cxcr7 Generates an Sdf1-Signaling Gradient across the Primordium

Next, we tested whether Cxcr7-mediated Sdf1a protein sequestration in the rear of the primordium is responsible for generating the Sdf1-signaling gradient across the primordium. Consistent with the variable migration defects observed in embryos deficient for either *cxcr7a* or *cxcr7b*, we find that Sdf1 signaling is increased specifically in the rear of the primordium in the absence of *cxcr7a* or *cxcr7b* activity compared to wild-type controls (Figures 4A and 4B, columns 1–3), resulting in a 31% or 40% reduction in the steepness of the Sdf1-signaling gradient across the primordium, respectively. These findings indicate that both CXCR7 orthologs contribute to the local clearance of Sdf1a protein and, thus, to the generation of the signaling gradient. Indeed, impairing both *cxcr7a* and *cxcr7b* activity in the same embryo increases Sdf1 signaling in the rear to levels that are normally only observed in the front of the primordium (Figures 4A and 4B, column 4). Importantly, this increase of Sdf1 signaling in the rear of the primordium of *cxcr7*-deficient embryos requires Sdf1a activity, as Sdf1 signaling in primordia of embryos lacking *cxcr7* and *sdf1a* resembles Sdf1 signaling in primordia of embryos mutant for *sdf1a* alone (Figures 4A and 4B, column 5). Conversely, in embryos that overexpress Cxcr7b from a heat-shock-inducible promoter, Sdf1-signaling is reduced throughout the primordium (Figures 4A and 4B, column 6). The absence of the Sdf1-signaling gradient in *cxcr7*-deficient primordia resembles the scenario in which Sdf1a is overexpressed globally (Figures 3H and 3I, column 5), whereas the low signaling levels observed across the primordium upon global Cxcr7b overexpression are similar to what we observed in *sdf1a* mutant primordia (Figures 3H and 3I, column 4), suggesting that Cxcr7 activity correlates inversely with Sdf1a levels. Furthermore, the abrogation of the Sdf1-signaling gradient in *cxcr7*-deficient embryos enables the relative quantification of the available Sdf1a levels outside of the primordium. In the absence of *cxcr7* activity, the mean FmemRed/FmemGreen in the primordium should correspond to the unaltered levels of Sdf1a on the stripe (C_0), and the mean FmemRed/FmemGreen in *sdf1a* mutant embryos should correspond to the absence of Sdf1a. Thus, the combined activities of Cxcr7a and Cxcr7b reduce Sdf1a beneath the rear of the primordium to 0.14 × C_0, whereas the front of the primordium perceives C_0. In summary, these observations demonstrate that Cxcr7a and Cxcr7b continuously sequester Sdf1a protein in the rear of the primordium. This results in an 86% reduction in the local concentration of Sdf1a in the rear of the primordium, which in turn generates the difference in chemical potential

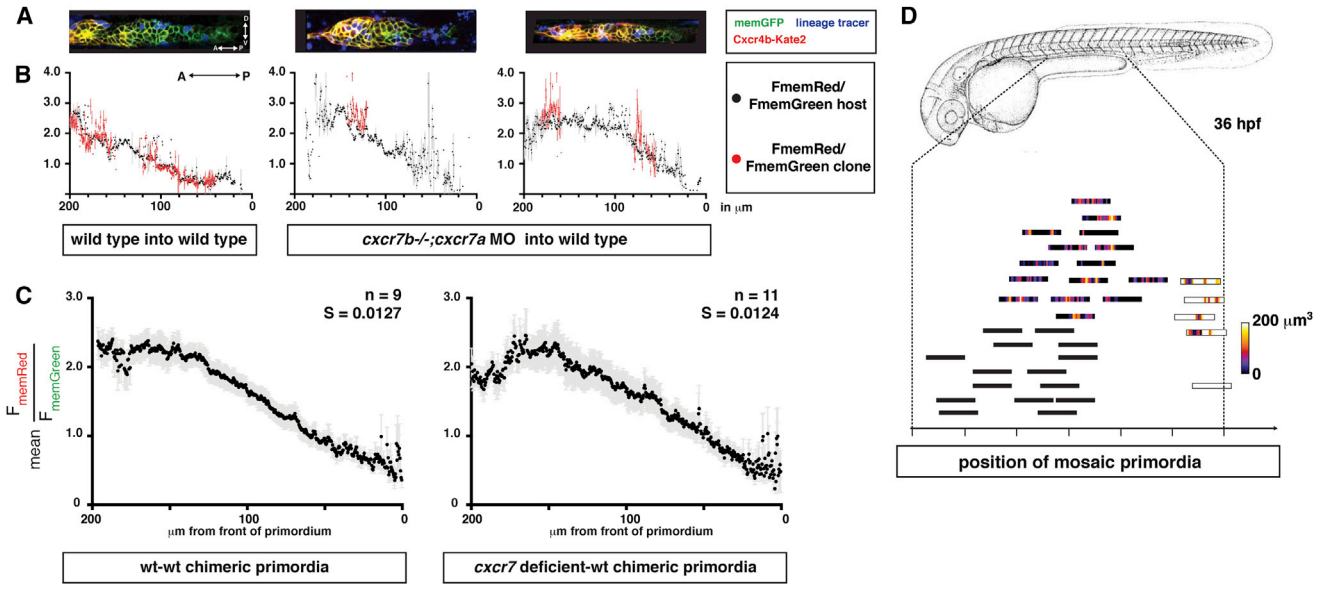

Figure 5. Cxcr7 Modifies the Sdf1-Signaling Gradient across the Primordium at the Tissue Level

(A) Single confocal slices through mosaic primordia in live 36 hpf embryos of the indicated genotypes.

(B) Quantification of mean FmemRed/FmemGreen of host cells (black dots, gray bars SEM) and donor cells (red dots, light-red bars SEM) across the anterior-posterior axis of primordia shown in (A).

(C) FmemRed/FmemGreen ratio on the host cells only across wild-type-wild-type and *cxcr7* deficient-wild-type chimeric primordia containing the Sdf1-signaling sensor. The front of the primordium is at 0 μm. Gray bars indicate SEM.

(D) Position of mosaic primordia compared to *cxcr7b* mutant (black rectangles) and wild-type primordia (white rectangle). The amount (heat map in μm^3) and position of clonal tissue across 150 μm from the front of the schematized primordia is indicated.

See also Table S1.

required for the formation of a linear gradient of the attractant along the migration route, which is essential for proper primordium migration.

Cxcr7 Shapes the Sdf1-Signaling Gradient on the Tissue Level

Cxcr7 could sculpt the chemokine gradient across the primordium through local competition with Cxcr4b for Sdf1a protein on the cell membranes of individual cells or through global chemokine clearance in the rear of the primordium. To distinguish between these possibilities, we used cell transplantation to generate chimeric primordia composed of wild-type and *cxcr7*-deficient cells and compared the FmemRed/FmemGreen ratios within and outside the clones. Placement of *cxcr7*-deficient cells in the rear of a wild-type primordium does not result in increased internalization of Cxcr4b-Kate2 selectively in the *cxcr7*-deficient clones when compared to adjacent wild-type cells or control chimeras (Figures 5A and 5B). This indicates that, although Cxcr7a and Cxcr7b clear Sdf1a protein locally, the reduction of Sdf1 signaling in the rear of the primordium is generated at the level of the tissue rather than the individual cell.

Supplying Cxcr7 Underneath the Rear of the Primordium Restores the Signaling Gradient and Primordium Migration in *cxcr7*-Deficient Embryos

If Cxcr7's sole function is to clear Sdf1a protein from underneath the rear of the primordium, then resupplying Cxcr7 specifically underneath the rear of *cxcr7*-deficient primordia should restore Sdf1-signaling gradient formation and primordium migration. To test this idea, we ectopically expressed *cxcr7b* in the posterior lateral line nerve—a nerve whose axons closely track the rear of the migrating primordium through GDNF signaling (Schuster et al., 2010)—in *cxcr7*-deficient embryos. In such embryos, the magnitude of the Sdf1-signaling gradient across the primordium is restored to 85% of the wild-type levels (Figure 4B, column 7), and the primordium migrates on average halfway down the trunk and tail (Figures 1D and S6C). This is in contrast to *cxcr7*-deficient control embryos in which the Sdf1-signaling gradient is shallower (Figure 4, column 4) and primordium migration is almost completely impaired (Figures 1D and S6C). These observations indicate that Cxcr7 is not necessarily required within the primordium itself and is sufficient for Sdf1-signaling gradient generation and primordium migration when supplied beneath the rear of the primordium.

A Steady-State Sdf1-Signaling Gradient Guides the Migrating Primordium

Given sufficient time, the shape and amplitude of signaling molecule gradients will reach steady state in many scenarios (Müller et al., 2013; Wartlick et al., 2009). However, signaling processes often occur within a few hours, and it is unclear whether gradients can reach steady state within such short time frames and, in turn, if cells interpret pre-steady-state or steady-state signaling gradients in vivo. To address these questions, we analyzed the formation of the Sdf1-signaling gradient over time. A brief heat-shock-induced pulse of global Sdf1a protein

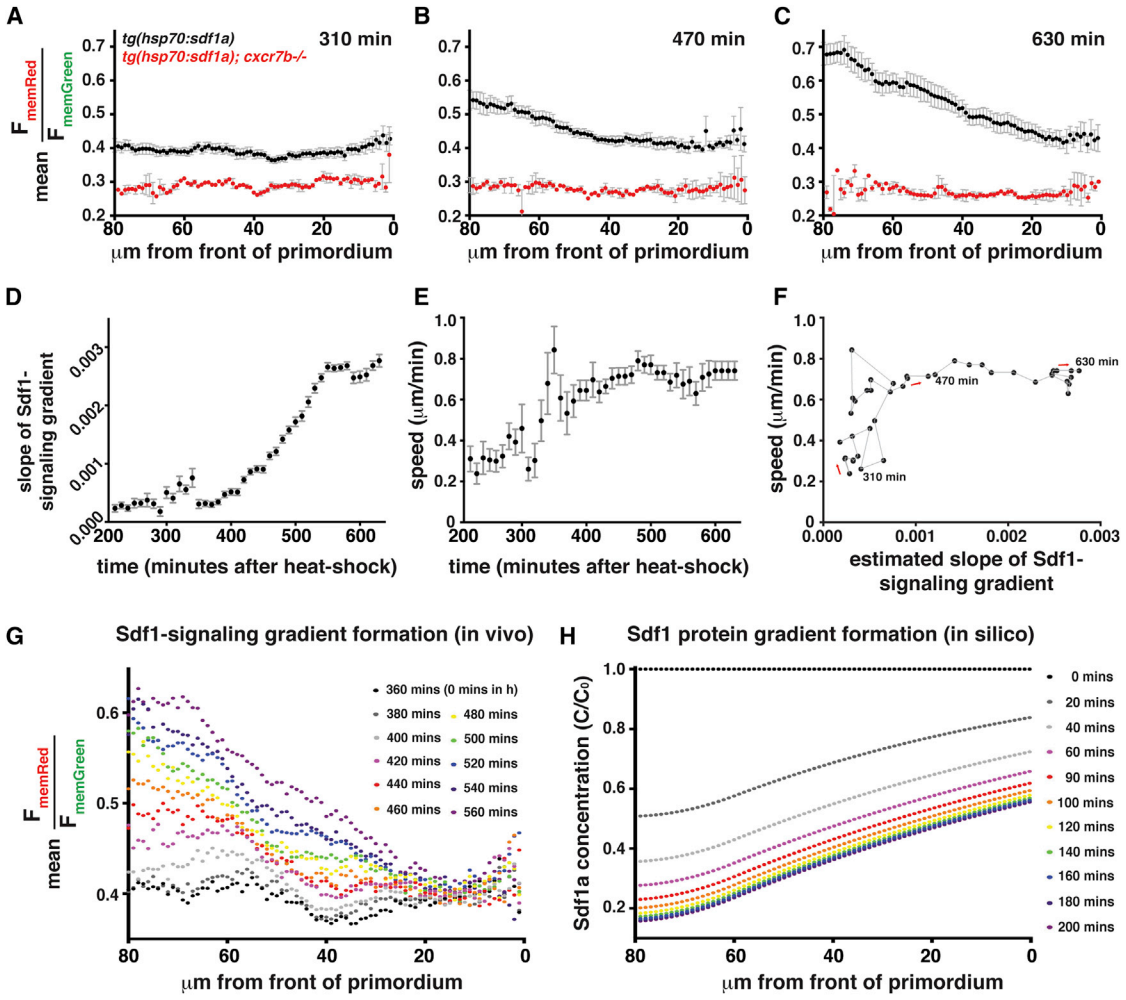

Figure 6. Kinetics of Sdf1-Signaling Gradient Formation

(A–C) Mean FmemRed/FmemGreen along the anterior-posterior axis in *tg(hsp70:sdf1a)* (black dots, n = 8) and *tg(hsp70:sdf1a);cxcr7b*$^{-/-}$ (red dots, n = 2) at the indicated number of minutes after induction of a pulse of global Sdf1a expression. The front of the primordium is at 0 μm. Gray bars indicate SEM.

(D–F) Relationships of the slope of the gradient, speed of the primordium, and time (n = 8). In (D) and (E), solid black circles indicate mean, and gray bars indicate SEM. In (F), the gray line connects the data points in chronological order, as indicated by red arrows.

(G and H) Sdf1-signaling gradient formation in vivo (G) and Sdf1a protein gradient formation predicted in silico (H). 0 min (post-heat-shock) in (H) roughly corresponds to 360 min in (G).

See also Figure S7.

expression causes internalization of Cxcr4b-Kate2 throughout the primordium, flattens the Sdf1-signaling gradient, and decelerates the primordium (Movie S6, top). The gradient begins to recover ~5–6 hr after the heat shock and converges to the linear shape that is observed across wild-type primordia (Figures 6A–6C and S7 and Movies S6, top, and S7). Concurrent with recovery of the gradient, the rounded primordium elongates and resumes normal migration (Movie S6, top). Analysis of this recovery reveals a sequence of three distinct states of Sdf1 signaling across the primordium that result in re-establishment of the signaling gradient. At ~5 hr post-heat-shock, the Sdf1-signaling gradient across the primordium is absent (Figures 6A and S7A and Movie S7). At ~7–8 hr post-heat-shock, Sdf1-signaling is reduced specifically in the rear of the primordium, resulting in a nonlinear, sigmoidal Sdf1-signaling gradient (Figures 6B and S7B and Movie S7). Over the next ~2 hr, this sigmoidal gradient equilibrates across the primordium to yield a steeper, linear gradient that resembles the gradient observed in wild-type primordia and remains relatively stable until the end of the imaging period (Figures 6C, 6G, and S7C and Movie S7), indicating that it has reached a steady state. Importantly, the time required for re-establishment of the Sdf1-signaling gradient across the primordium depends on *cxcr7* activity. In *cxcr7b* mutant embryos, a genetic scenario in which the slope of the Sdf1-signaling gradient across the primordium is already reduced by 40% even before heat shock (Figures 4A and 4B, column 3), the gradient remains flat ~10 hr following a similar pulse of global Sdf1a protein expression (Figures 6A–6C and Movies S6, bottom, and S7).

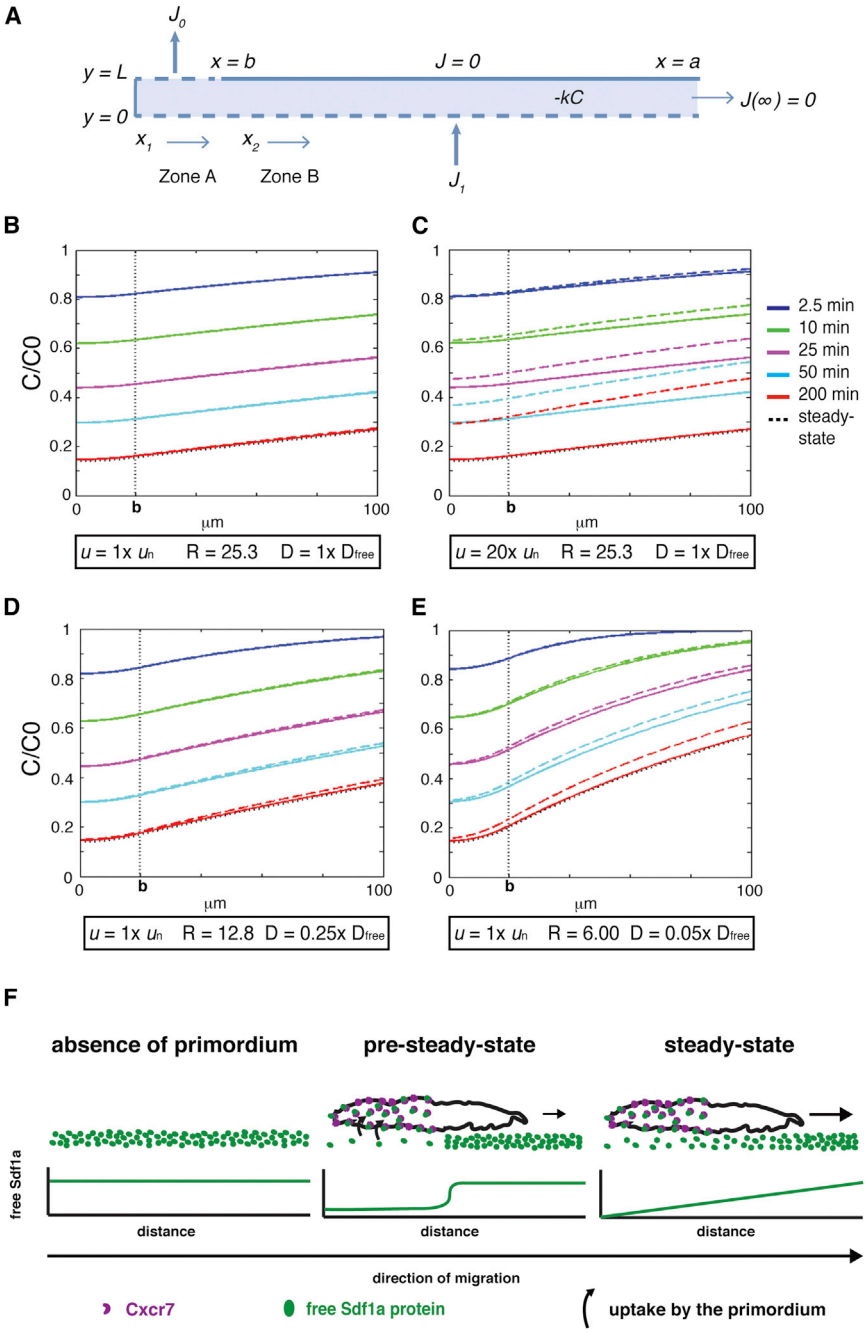

Figure 7. Model for the Evolution of Chemokine Gradient with Different Values of Velocity and Effective Diffusion Coefficient

(A) Model. L, thickness of chemokine reservoir; k, Sdf1 degradation rate in reservoir; J_0, flux into the region of primordium absorbing chemokine ($b > x > 0$, $y = L$ with $b = 20$ μm); J_1, flux of Sdf1 from producing cells ($x > 0$, $y = 0$); C, concentration of chemokine; and C_0 initial value of C at time $t = 0$. The gradient is sensed over the surface of $a > x > b$, $y = L$ wherein a is 100 μm and there is no flux over this region. Two zones are defined: zone A represents $b > x_1 > 0$, and zone B represents $a > x_2 > b$. In (B)–(E), the colored solid lines correspond to the gradients calculated with velocity of primordium velocity (u) = 0, and the colored dashed lines are calculated with the specified u. Each gradient is calculated at the indicated time, assuming that $C/C_0 = 1$ at $t = 0$. The dotted black line indicates steady state. k is fixed at 0.0003 s^{-1}. $R = J_0/J_1$ is the ratio of flux values chosen so that the steady-state baseline value of C under the sink ($x = 0$) corresponds to the measured value of 0.14 C_0.

(B–E) Simulations with different u and effective diffusion coefficient (D) expressed as multiples of measured u_n (0.7 μm min^{-1}) and D_{free} (100 μm^2 s^{-1}; Veldkamp et al., 2005).

(F) Model for chemokine-signaling gradient by the primordium. In the pre-steady-state, sequestration of Sdf1a protein by Cxcr7 decreases Sdf1a protein beneath the trailing half of the primordium, resulting in reduced chemokine signaling in the rear. Diffusion from areas of higher Sdf1a protein concentration equilibrates the chemokine distribution across the primordium, resulting in a linear, stable signaling gradient.

Mathematical Modeling of Gradient Formation by a Moving Sink

The local sequestration of Sdf1a protein in the rear of the migrating primordium bears a superficial resemblance to the source-sink model described by Crick (1970). Crick showed that a freely diffusing molecule produced by a localized source and degraded by a localized sink should result in a linear gradient at steady state. Consistent with this prediction, the Sdf1-signaling gradient across wild-type primordia appears linear (Figure 3I, columns 1–3), and there is a sink in the rear of the primordium that locally degrades Sdf1a. In contrast to Crick's localized source model, however, the stripe of *sdf1a*-expressing cells generates a spatially distributed reservoir of Sdf1a along the migration route. To test whether such a distributed source might provide similar results to Crick's model, we modeled these dynamics under two assumptions. First, the flux of Sdf1a from a distributed source of chemokine-producing cells is balanced by its degradation to yield a constant reservoir of Sdf1a. Second, the rear of the primordium clears Sdf1a at a constant flow rate (Figure 7A). Initially, we used a value of 100 μm^2 s^{-1} for the diffusion coefficient of Sdf1 (i.e., the free diffusion coefficient; see Extended Experimental Procedures). Consistent with our analysis of the Sdf1-signaling gradient kinetics and the estimated Peclet number of 0.012 (a measure for whether a system is dominated by diffusion or flow), this model predicts that the primordium migration velocity of ~0.7 μm min^{-1} does not contribute significantly to the formation of the gradient (Figures 7B and 7C). Moreover, this model shows that a stable, linear, gradient can form in 0.5–3 hr and is only

slightly perturbed by the motion of the primordium (Figures 7B–7E). However, the model predicts a shallower signaling gradient across the primordium (Figure 7B) than what we observe in vivo (Figure 3I, column 1–3), perhaps reflecting hindered Sdf1a diffusion mediated by molecules in the extracellular matrix that can bind the chemokine, a scenario that is known to reduce the effective diffusion coefficient (Crank, 1975, Chapter 14). Three of our observations are consistent with this idea. First, Sdf1a protein is produced by the stripe of chemokine-expressing cells throughout the 20 hr migration period but does not diffuse to detectable levels into adjacent tissues (Movie S2), suggesting that Sdf1a protein is retained close to its source. Second, only 1% of the total Sdf1a-GFP protein on the stripe is sequestered through Cxcr7 in the rear of the primordium (Figure 2F). This suggests that a large fraction of the chemokine is bound to the extracellular matrix, a proposition that has also been put forward for other secreted signaling molecules (Müller et al., 2013). Importantly, prolonged global overexpression of Cxcr7b results in removal of 29% of the total Sdf1a-GFP protein from the stripe (Figure 2B), indicating that a larger fraction of Sdf1a protein than the 1% sequestered by the primordium is present, but not accessible to Cxcr7 in the rear of the primordium. Third, the kinetics of Sdf1 gradient formation are approximated by the model if the free diffusion coefficient of Sdf1 is reduced by a factor of between 4 and 20 (Figures 7D and 7E). Note that, even when the diffusion coefficient is reduced by 20, the Peclet number is still 0.24. In summary, this modeling analysis supports the plausibility of a scenario in which a localized Cxcr7-mediated sink activity combined with hindered Sdf1a protein diffusion (i.e., reduced diffusion coefficient) from a distributed source and degradation mechanism generates a quasi-linear and stable Sdf1-signaling gradient across the primordium (Extended Experimental Procedures).

Steepness of Sdf1-Signaling Gradient Correlates with Efficient Primordium Migration

Theoretical considerations and in vitro experiments have suggested that increasing the steepness of an attractant gradient can promote directionality and motility (Fisher et al., 1989; Hatzikirou and Deutsch, 2008; Keller and Segel, 1971; Parent and Devreotes, 1999). To test this model in vivo, we followed the recovery of the Sdf1-signaling gradient and primordium migration speed following exposure to a global pulse of Sdf1a. By comparing the average slope of the signaling gradient and the average speed of the primordium (Figures 6D–6F), we found that, when the slope of the Sdf1-signaling gradient is at or above ~46% of its steady-state value (470 min in Figure 6F), the speed of the primordium stabilizes at ~0.7 μm/min (Figure 6F), which is similar to the speed observed in wild-type primordia (Haas and Gilmour, 2006). During this recovery period, the Sdf1-signaling gradient increases fairly linearly (Figure 6D) until it stabilizes at steady state. When the gradient is less than ~46% of the steady-state value, however, both the speed and directionality of the primordium are unpredictable (Figure 6F), with primordia either stalling or exhibiting serpentine movement rather than straight migration. Importantly, shifting the gradient to higher ratios by low-dose Sdf1a morpholino injections without changing its slope (Figure 3C, left) does not affect primordium migration (Figure 3C, right). These observations are consistent with the idea that it is the steepness of an attractant gradient rather than the absolute amount of signaling that instructs both speed and directionality of migration in vivo.

DISCUSSION

Guidance of Migrating Cells by Shallow Attractant Gradients

In vitro studies using Dictyostelium and neutrophils have shown that individually migrating cells require at least a 3% difference in concentration between the front and the back of the cell for efficient directional migration (Fisher et al., 1989; Mato et al., 1975). This is similar to the 7% difference in Sdf1 signaling observed across the front to the back of a cell in the lateral line primordium, suggesting that shallow gradients are sufficient for efficient directional migration both in vitro and in vivo. Because most scenarios involving a local attractant source yield nonlinear gradients whose slope is shallow far from the source and steeper closer to the source (Wartlick et al., 2009), the ability of cells to detect small differences in attractant concentration is essential for migration toward the attractant source from a distance.

Collectively migrating cells can potentially compare differences in attractant concentration sensed by cells at the front and at the rear of the collective to polarize the tissue toward higher attractant concentrations (Rørth, 2007). The induction of polarity across collectively migrating border cells in flies by local activation of Rac (Wang et al., 2010) and the promotion of migration in primordia with a few wild-type cells in an otherwise cxcr4b mutant primordium (Haas and Gilmour, 2006) support this idea. However, reducing the difference in Sdf1 signaling across a cell within the primordium to 3% results in inefficient migration and stalling of the primordium, even though there still exists a 40% difference in Sdf1 signaling from the front to back across the primordium in *cxcr7b* mutant embryos. These observations suggest that either a 3% difference in signaling across cells might be too low to induce polarity across the primordium or, alternatively, that the primordium might not compare concentrations of the attractant across the collective to enhance its ability to detect attractant gradients.

Kinetics and Dynamics of Signaling Gradients

Signaling molecules disperse away from their source through a complex environment to pattern a field of cells or to provide guidance to migrating cells. The signaling range depends on the time that the signaling molecules have to disperse and the ability of the signaling molecules to move through the tissue (Müller and Schier, 2011). For many scenarios with constant production, diffusion, and clearance rates, the distribution of signaling molecules will converge toward a stable gradient (constant amplitude and shape) over time (Müller et al., 2013; Wartlick et al., 2009). Measurements of the total pool of fluorescently tagged and overexpressed signaling molecules indicate that it takes 30 min (in the case of nodal [Müller et al., 2012]) to 3–4 hr (in the cases of FGF [Yu et al., 2009] and dpp [Entchev et al., 2000; Teleman and Cohen, 2000]) for the signaling gradient to reach steady state. This is similar to the time that it takes for the signaling gradient of untagged, endogenous Sdf1 to converge toward

steady state, given that the distribution of the pool of total signaling molecules and the pool of actively signaling molecules do not necessarily need to display similar gradient kinetics.

The movement of signaling molecules through tissues is impeded by obstacles that increase the path length of the moving molecule and by transient binding to the extracellular matrix. This reduces the global diffusivity of the signaling molecule and increases the time that it takes for the gradient to converge toward steady state (Müller et al., 2013; Crank, 1975). The FGF gradient in the early zebrafish embryo, for example, approaches steady state over a period of 3–4 hr instead of less than an hour as predicted for freely diffusing FGF, suggesting that the movement of FGF is hindered by transient binding to extracellular molecules, such as proteoglycans (Duchesne et al., 2012; Müller et al., 2013). Similarly, the shape of the gradient of Sdf1 suggests that the chemokine is hindered in its diffusivity, a supposition supported by the observation that only a small fraction of the total Sdf1a protein pool actively participates in signaling. Although this might depend on the signaling molecule and the tissue context, these observations are consistent with the idea that a large fraction of the signaling molecules is bound to extracellular molecules at any given time, and only a small fraction is locally available to engage in signaling.

Self-Generated Attractant Gradients

The primordium is born as a polarized tissue with a rosette in its rear that will be deposited later as the first neuromast (Nechiporuk and Raible, 2008). Shortly afterward, the rear of the primordium starts expressing *cxcr7b* (Breau et al., 2012; Dambly-Chaudière et al., 2007). Although the molecular mechanism leading to the expression of *cxcr7b* in the rear is unknown, this restricted expression polarizes the primordium molecularly. Three conflicting models have been proposed about how Cxcr7b activity in the rear could provide directionality to the migrating primordium. In the first model, Cxcr7b activity is thought to repress the expression of *cxcr4b* in the rear, and Cxcr4b activity in the front is thought to repress *cxcr7b* expression in the front of the primordium. This cross-repression would cause Cxcr4b activity to become graded across the primordium, with more Cxcr4b available for signaling in the front than in the back (Dambly-Chaudière et al., 2007). In the second model, Cxcr7b is thought not to regulate *cxcr4b* expression but instead to elicit a response that is distinct from Cxcr4b upon Sdf1a activation. This response is thought to endow cells in the rear of the primordium with a different migratory behavior than cells in the front (Valentin et al., 2007). In the third model, Cxcr7b activity was proposed to internalize Sdf1 protein in the rear of the primordium, which in turn was postulated to generate a gradient of Sdf1 protein across the primordium, which the primordium would follow (Raz and Mahabaleshwar, 2009; Weijer, 2009). Our expression analysis of the transgenic reporters is consistent with the second model in which Cxcr4b and Cxcr7b do not regulate each other's expression (Figure 1B). However, the findings that Cxcr7 expression both in the rear primordium and near the rear of the primordium similarly lead to the formation of a Sdf1-signaling gradient and primordium migration (Figures 1D, 4B, 5D, and S6C) indicate that Cxcr7 acts not as a signaling receptor but, rather, as a chemokine clearance receptor during primordium migration. This is consistent with the third model, in which Cxcr7 acts as a sink for Sdf1 in the rear of the primordium, generates an Sdf1-signaling gradient across the primordium, and propels its migration along a uniform source of attractant (Figure 7F), but it is inconsistent with a role of Cxcr7 in signaling in the rear of the primordium, as postulated in the second model.

It is conceivable that ligand sequestration by a subset of cells in a migrating cluster represents a more general mechanism of generating, maintaining, or enhancing a gradient of an attractant —or any signaling molecule—in order to provide directional and/or positional information to cells and tissues. Key to this mechanism is the ability to change the availability of an extracellular signaling molecule, which depends on the signaling molecule's concentration, the number of sink cells, and the rate of ligand sequestration. Many other tissues such as sprouting blood vessels, epithelia, and metastasizing tumors exhibit collective migration (Friedl and Gilmour, 2009; Montell, 2008; Rørth, 2009). Thus, a migrating collective modulating the availability of its own guidance cue may represent an elegant mechanism of cell guidance.

EXPERIMENTAL PROCEDURES

Sdf1a-GFP and Sdf1-Signaling Sensor Transgenics

The Sdf1-signaling sensor and the Sdf1a-GFP fusion constructs were generated using recombineering of a bacterial artificial chromosome (BAC) spanning the *cxcr4b* and *sdf1a* genomic loci, respectively, and transgenic zebrafish were obtained by co-injecting BAC DNA and *tol2* transposase mRNA into one-cell-stage embryos. See also Extended Experimental Procedures.

Immunohistochemistry, Embryonic Manipulations, and Transgenesis

In situ hybridization was conducted as previously described (Thisse and Thisse, 2008). Antibody stainings were detected chromogenically with DAB or fluorescently with Cy3-, Alexa488-, or Alexa647-conjugated secondary antibodies. Mosaic embryos containing either the Sdf1-signaling sensor or *tg(hsp70:sdf1a)* and *tg(cldnB:lyn$_2$GFP)* were generated through cell transplantation. See also Extended Experimental Procedures.

Microscopy and Image Processing

For live imaging, the primordium was imaged using a Leica SP5 II confocal laser scanning microscope. Quantification of Sdf1a-GFP on the stripe and FmemRed/FmemGreen ratios for each voxel representing part of a cell membrane in the primordium were calculated using ImageJ software. See also Extended Experimental Procedures.

SUPPLEMENTAL INFORMATION

Supplemental Information includes Extended Experimental Procedures, seven figures, one table, seven movies, and five data files and can be found with this article online at http://dx.doi.org/10.1016/j.cell.2013.09.046.

ACKNOWLEDGMENTS

We thank J. Torres-Vazquez, F. Schnorrer, J. Nance, R. Lehmann, R. Cinalli, J. Hubbard, and J. Treisman for critical comments; D. Gilmour, P. Krieg, and A.J. Hudspeth for reagents; F. Fuentes for excellent fish care; K. Cadwell and G. David for cell lines; M. Stadtfeld for recombinant LIF; and A. Sfeir and M. Tahiliani for advice and reagents for tissue culture experiments. For providing the zebrafish knockout allele *cxcr7b^{sa16}*, we thank E. Busch-Nentwich and D. Stemple, Sanger Institute Zebrafish Mutation Resource, sponsored by the Wellcome Trust (grant number WT 077047/Z/05/Z). This work was supported

by NIH grants NS069839 (H.K.), NS28642 (C.N.), and HD007520 (S.W.L.) and by an American Heart Association fellowship 12POST12060278 (G.V.).

Received: June 10, 2013
Revised: August 19, 2013
Accepted: September 24, 2013
Published: October 10, 2013

REFERENCES

Affolter, M., and Caussinus, E. (2008). Tracheal branching morphogenesis in Drosophila: new insights into cell behaviour and organ architecture. Development *135*, 2055–2064.

Aman, A., and Piotrowski, T. (2010). Cell migration during morphogenesis. Dev. Biol. *341*, 20–33.

Boldajipour, B., Mahabaleshwar, H., Kardash, E., Reichman-Fried, M., Blaser, H., Minina, S., Wilson, D., Xu, Q., and Raz, E. (2008). Control of chemokine-guided cell migration by ligand sequestration. Cell *132*, 463–473.

Breau, M.A., Wilson, D., Wilkinson, D.G., and Xu, Q. (2012). Chemokine and Fgf signalling act as opposing guidance cues in formation of the lateral line primordium. Development *139*, 2246–2253.

Cai, H., and Devreotes, P.N. (2011). Moving in the right direction: how eukaryotic cells migrate along chemical gradients. Semin. Cell Dev. Biol. *22*, 834–841.

Crank, J. (1975). Mathematics of Diffusion (Oxford, UK: Oxford University Press).

Crick, F. (1970). Diffusion in embryogenesis. Nature *225*, 420–422.

Crump, M.P., Gong, J.H., Loetscher, P., Rajarathnam, K., Amara, A., Arenzana-Seisdedos, F., Virelizier, J.L., Baggiolini, M., Sykes, B.D., and Clark-Lewis, I. (1997). Solution structure and basis for functional activity of stromal cell-derived factor-1; dissociation of CXCR4 activation from binding and inhibition of HIV-1. EMBO J. *16*, 6996–7007.

Dambly-Chaudière, C., Cubedo, N., and Ghysen, A. (2007). Control of cell migration in the development of the posterior lateral line: antagonistic interactions between the chemokine receptors CXCR4 and CXCR7/RDC1. BMC Dev. Biol. *7*, 23.

David, N.B., Sapède, D., Saint-Etienne, L., Thisse, C., Thisse, B., Dambly-Chaudière, C., Rosa, F.M., and Ghysen, A. (2002). Molecular basis of cell migration in the fish lateral line: role of the chemokine receptor CXCR4 and of its ligand, SDF1. Proc. Natl. Acad. Sci. USA *99*, 16297–16302.

Duchesne, L., Octeau, V., Bearon, R.N., Beckett, A., Prior, I.A., Lounis, B., and Fernig, D.G. (2012). Transport of fibroblast growth factor 2 in the pericellular matrix is controlled by the spatial distribution of its binding sites in heparan sulfate. PLoS Biol. *10*, e1001361.

Entchev, E.V., Schwabedissen, A., and González-Gaitán, M. (2000). Gradient formation of the TGF-beta homolog Dpp. Cell *103*, 981–991.

Fisher, P.R., Merkl, R., and Gerisch, G. (1989). Quantitative analysis of cell motility and chemotaxis in Dictyostelium discoideum by using an image processing system and a novel chemotaxis chamber providing stationary chemical gradients. J. Cell Biol. *108*, 973–984.

Friedl, P., and Gilmour, D. (2009). Collective cell migration in morphogenesis, regeneration and cancer. Nat. Rev. Mol. Cell Biol. *10*, 445–457.

Ghysen, A., and Dambly-Chaudière, C. (2007). The lateral line microcosmos. Genes Dev. *21*, 2118–2130.

Haas, P., and Gilmour, D. (2006). Chemokine signaling mediates self-organizing tissue migration in the zebrafish lateral line. Dev. Cell *10*, 673–680.

Hatzikirou, H., and Deutsch, A. (2008). Cellular automata as microscopic models of cell migration in heterogeneous environments. Curr. Top. Dev. Biol. *81*, 401–434.

Keller, E.F., and Segel, L.A. (1971). Model for chemotaxis. J. Theor. Biol. *30*, 225–234.

Kicheva, A., Pantazis, P., Bollenbach, T., Kalaidzidis, Y., Bittig, T., Jülicher, F., and González-Gaitán, M. (2007). Kinetics of morphogen gradient formation. Science *315*, 521–525.

Kimmel, C.B., Ballard, W.W., Kimmel, S.R., Ullmann, B., and Schilling, T.F. (1995). Stages of embryonic development of the zebrafish. Dev. Dyn. *203*, 253–310.

Li, Q., Shirabe, K., and Kuwada, J.Y. (2004). Chemokine signaling regulates sensory cell migration in zebrafish. Dev. Biol. *269*, 123–136.

Marchese, A., and Benovic, J.L. (2001). Agonist-promoted ubiquitination of the G protein-coupled receptor CXCR4 mediates lysosomal sorting. J. Biol. Chem. *276*, 45509–45512.

Marchese, A., Raiborg, C., Santini, F., Keen, J.H., Stenmark, H., and Benovic, J.L. (2003). The E3 ubiquitin ligase AIP4 mediates ubiquitination and sorting of the G protein-coupled receptor CXCR4. Dev. Cell *5*, 709–722.

Mato, J.M., Losada, A., Nanjundiah, V., and Konijn, T.M. (1975). Signal input for a chemotactic response in the cellular slime mold Dictyostelium discoideum. Proc. Natl. Acad. Sci. USA *72*, 4991–4993.

Minina, S., Reichman-Fried, M., and Raz, E. (2007). Control of receptor internalization, signaling level, and precise arrival at the target in guided cell migration. Curr. Biol. *17*, 1164–1172.

Montell, D.J. (2003). Border-cell migration: the race is on. Nat. Rev. Mol. Cell Biol. *4*, 13–24.

Montell, D.J. (2008). Morphogenetic cell movements: diversity from modular mechanical properties. Science *322*, 1502–1505.

Müller, P., and Schier, A.F. (2011). Extracellular movement of signaling molecules. Dev. Cell *21*, 145–158.

Müller, P., Rogers, K.W., Jordan, B.M., Lee, J.S., Robson, D., Ramanathan, S., and Schier, A.F. (2012). Differential diffusivity of Nodal and Lefty underlies a reaction-diffusion patterning system. Science *336*, 721–724.

Müller, P., Rogers, K.W., Yu, S.R., Brand, M., and Schier, A.F. (2013). Morphogen transport. Development *140*, 1621–1638.

Nechiporuk, A., and Raible, D.W. (2008). FGF-dependent mechanosensory organ patterning in zebrafish. Science *320*, 1774–1777.

Parent, C.A., and Devreotes, P.N. (1999). A cell's sense of direction. Science *284*, 765–770.

Rajagopal, S., Kim, J., Ahn, S., Craig, S., Lam, C.M., Gerard, N.P., Gerard, C., and Lefkowitz, R.J. (2009). Beta-arrestin- but not G protein-mediated signaling by the "decoy" receptor CXCR7. Proc. Natl. Acad. Sci. USA *107*, 628–632.

Raz, E., and Mahabaleshwar, H. (2009). Chemokine signaling in embryonic cell migration: a fisheye view. Development *136*, 1223–1229.

Rørth, P. (2007). Collective guidance of collective cell migration. Trends Cell Biol. *17*, 575–579.

Rørth, P. (2009). Collective cell migration. Annu. Rev. Cell Dev. Biol. *25*, 407–429.

Rørth, P. (2011). Whence directionality: guidance mechanisms in solitary and collective cell migration. Dev. Cell *20*, 9–18.

Sánchez-Alcañiz, J.A., Haege, S., Mueller, W., Pla, R., Mackay, F., Schulz, S., López-Bendito, G., Stumm, R., and Marín, O. (2011). Cxcr7 controls neuronal migration by regulating chemokine responsiveness. Neuron *69*, 77–90.

Schuster, K., Dambly-Chaudière, C., and Ghysen, A. (2010). Glial cell line-derived neurotrophic factor defines the path of developing and regenerating axons in the lateral line system of zebrafish. Proc. Natl. Acad. Sci. USA *107*, 19531–19536.

Swaney, K.F., Huang, C.-H., and Devreotes, P.N. (2010). Eukaryotic chemotaxis: a network of signaling pathways controls motility, directional sensing, and polarity. Annu. Rev. Biophys. *39*, 265–289.

Teleman, A.A., and Cohen, S.M. (2000). Dpp gradient formation in the Drosophila wing imaginal disc. Cell *103*, 971–980.

Thisse, C., and Thisse, B. (2008). High-resolution in situ hybridization to whole-mount zebrafish embryos. Nat. Protoc. *3*, 59–69.

Valentin, G., Haas, P., and Gilmour, D. (2007). The chemokine SDF1a coordinates tissue migration through the spatially restricted activation of Cxcr7 and Cxcr4b. Curr. Biol. *17*, 1026–1031.

Veldkamp, C.T., Peterson, F.C., Pelzek, A.J., and Volkman, B.F. (2005). The monomer-dimer equilibrium of stromal cell-derived factor-1 (CXCL 12) is altered by pH, phosphate, sulfate, and heparin. Protein Sci. *14*, 1071–1081.

Wang, X., He, L., Wu, Y.I., Hahn, K.M., and Montell, D.J. (2010). Light-mediated activation reveals a key role for Rac in collective guidance of cell movement in vivo. Nat. Cell Biol. *12*, 591–597.

Wartlick, O., Kicheva, A., and González-Gaitán, M. (2009). Morphogen gradient formation. Cold Spring Harb. Perspect. Biol. *1*, a001255–a001255.

Weber, M., Hauschild, R., Schwarz, J., Moussion, C., de Vries, I., Legler, D.F., Luther, S.A., Bollenbach, T., and Sixt, M. (2013). Interstitial dendritic cell guidance by haptotactic chemokine gradients. Science *339*, 328–332.

Weijer, C.J. (2009). Collective cell migration in development. J. Cell Sci. *122*, 3215–3223.

Yu, S.R., Burkhardt, M., Nowak, M., Ries, J., Petrášek, Z., Scholpp, S., Schwille, P., and Brand, M. (2009). Fgf8 morphogen gradient forms by a source-sink mechanism with freely diffusing molecules. Nature *461*, 533–536.

EXTENDED EXPERIMENTAL PROCEDURES

Zebrafish Strains

Embryos were staged as previously described (Kimmel et al., 1995). *cxcr4b*^{t26035} (Knaut et al., 2003), *sdf1a*^{t30516} (Valentin et al., 2007) and *cxcr7b*^{sa16} (Kettleborough et al., 2013) homozygous mutant embryos were generated by inbreeding homozygous adults, crossing homozygous adults with heterozygous adults or inbreeding heterozygous adults. Mutant, heterozygous and wild-type embryos were distinguished through PCR-amplification of the mutated locus and sequencing or restriction digest with NlaIV (New England Biolabs) for *sdf1a* and HpyAV (New England Biolabs) for *cxcr4b*. *Tg(cldnB:lyn$_2$GFP)* (Haas and Gilmour, 2006), *tg(hsp70:sdf1a)* (Knaut et al., 2005) and *tg(hsp70:cxcr7b)* (Lewellis et al., 2013) embryos were generated by crossing heterozygous transgenic adults to wild-type adults. Transgenic embryos were identified by GFP fluorescence, in situ hybridization against *sdf1a* and *cxcr7b* mRNA or by PCR-amplification of the transgene using the following primers:

tg(hsp70:sdf1a) genotyping primers:
Outer PCR: TGAGCATAATAACCATAAATACTA and TCTGTGGGACTGTGTTGACTGTGG
Nested PCR (using product of outer PCR as template): AGCAAATGTCCTAAATGAAT and TCTGTGGGACTGTGTTGACTGTGG
tg(hsp70:cxcr7b) genotyping primers:
Outer PCR: TGAGCATAATAACCATAAATACTA and GAGGCCAATGATGAAGAGGAAGAT
Nested PCR (using product of outer PCR as template): AGCAAATGTCCTAAATGAAT and CTCTGGCTGAAGGTGCTGTG

Generation of Transgenic Strains

For the Sdf1a-GFP transgene, the BAC clone CH73-199F2 was modified in two ways by recombineering. First, the Tol2 *(exon 4)-FRT-GalK-FRT-Tol2 (exon 1)-alpha-Crystallin-dsRed* cassette was inserted into the BAC replacing nucleotides 3008 to 3052 of the pTARBAC2 backbone using *GalK* as a selection marker. *GalK* was removed by Flippase-mediated recombination. The arms of homology were 231 bp and 242 bp fragments corresponding to nucleotides 2777 to 3007 and 3053 to 3294 of the pTARBAC2 backbone, respectively. These arms of homology were subcloned into a pBluescript vector to flank the *Tol2-alpha-crystallin-dsRed* targeting cassette. Second, the GFP coding sequence was inserted between the last amino acid and the stop codon of *sdf1a* using seamless GalK-mediated recombineering. The 51 bp and 46 bp of homology upstream and downstream of the *sdf1a* stop codon, respectively, were added to the GFP targeting cassette by PCR. The final BAC was characterized by restriction digest, PCR amplification and BAC-end sequencing. It was then purified with the nucleobond BAC 100 kit (Clontech) and coinjected with *tol2* transposase mRNA into one-cell-stage zebrafish embryos. Stable transgenic larvae were identified by out-crossing adults injected with the transgene and by raising larvae with red fluorescence in the lens from the transgenesis marker at 5 days postfertilization. The full name of this transgenic line is *tg(sdf1a:sdf1a-EGFP)p10*.

For the Sdf1-signaling sensor, the BAC clone DKEY-169F10 was modified in two ways by recombineering. First, the Tol2 *(exon 4)-FRT-GalK-FRT-Tol2 (exon 1)-alpha-Crystallin-dsRed* cassette was inserted into the BAC replacing nucleotides 729 to 760 of its pIndigo-356 backbone using *GalK* as a selection marker. *GalK* was removed by Flippase-mediated recombination. The arms of homology were 320 bp fragments corresponding to nucleotides 409 to 728 and 761 to 1080 of the pIndigo-356 backbone, respectively. These arms of homology were subcloned into a pBluescript vector to flank the *Tol2-alpha-crystallin-dsRed* targeting cassette. Second, a cassette consisting of *Kate2*, an IRES from the encephalomyocarditis virus, and *EGFP-CaaX* followed by *FRT-kanamycin-FRT* flanked by 1457 bp and 812 bp of homology upstream and downstream of the *cxcr4b* stop codon, respectively, was inserted between the last amino acid and the stop codon of *cxcr4b* using the kanamycin resistance gene as a selection marker. The kanamycin resistance gene was removed by Flippase-mediated recombination. The final BAC was characterized by restriction digest, PCR amplification and BAC-end sequencing. It was then purified with the nucleobond BAC 100 kit (Clontech) and coinjected with *tol2* transposase mRNA into one-cell-stage zebrafish embryos. Stable transgenic larvae were identified by out-crossing adults injected with the transgene and by raising larvae with red fluorescence in the lens from the transgenesis marker at 5 days postfertilization. The full name of this transgenic line is *tg(cxcr4b:cxcr4b-Kate2-IRES-EGFP-CaaX)p7*. The Sdf1-signaling sensors with inverted color combination were generated as described above but fusing *cxcr4b* to GFP followed by an IRES driving membrane-tethered *Kate2*. The abbreviations of these transgenic lines are *Sdf1 sensorGRp1* and *Sdf1 sensorGRp7* and the full name of these transgenic lines are *tg(cxcr4b:cxcr4b-EGFP-IRES-Kate2-CaaX)p1* (Lewellis et al., 2013) and *tg(cxcr4b:cxcr4b-EGFP-IRES-Kate2-CaaX)p7,* respectively.

For mis-expressing *cxcr7b* in the posterior lateral line nerve, *cxcr7b-ires-Cerulean-CaaX* was assembled by stitching PCR and cloned into pME (Invitrogen) and the 3.8 kb *tubb2b* promoter (GenBank: EF989124.1, gift from Paul Krieg) was cloned into p5E (Invitrogen). Using gateway recombination the *tubb2b* promoter was placed upstream of *cxcr7b-ires-CFP-CaaX* and a SV40pA signal in pDestTol2pA2 (Kwan et al., 2007). The plasmid was coinjected with *tol2* transposase mRNA into one-cell-stage zebrafish embryos. Stable transgenic fish were identified by out-crossing adults injected with the transgene and raising larvae from fish whose offspring were identified to express Cerulean in the posterior lateral line nerve by immunostaining. The full name of this transgenic line is *tg(tubb2b:cxcr7b-IRES-CFP-CaaX)p3*. Transgenic embryos were identified by anti-CFP antibody staining or PCR using the following primers:

tg(tubb2b:cxcr7b-IRES-CFP-CaaX) genotyping primers:
Outer PCR: GTCTGAGACTGAATACTCAGCC and GAAAGACCCCTAGGAATGCTCG
Nested PCR (using product of outer PCR as template): GGAAAACCAGGGACCATTATGA and AAGAAGACAGGGCCAGGTTTCC

Fluorescent Imaging of Sdf1a-GFP

For fluorescent imaging of Sdf1a-GFP *tg*(*sdf1a:sdf1a-GFP*), embryos were fixed at 36 hpf and stained for GFP and ClaudinB (see below for details). The stained embryos were mounted on slides and z-stacks were collected with a Leica 63x oil immersion objective (NA 1.4) on a Leica SP5 II confocal microscope equipped with HyD detectors. All z-stacks were collected with identical microscope settings in photon-counting mode. For imaging embryos overexpressing Cxcr7b, *tg(hsp70:cxcr7b)* embryos were raised at 28°C to 31 hpf. At this time the embryos were heat shocked for 1 hr at 37°C, raised at 28°C to 36 hpf, fixed and stained. Embryos were genotyped by PCR as described above.

Quantification of Sdf1a-GFP Immunofluorescence and Sdf1a-GFP Puncta Inside of the Primordium

Using intensity thresholding and Gaussian blur in ImageJ (NIH), a mask was applied to the image based on the ClaudinB channel, which was refined to include only voxels within the primordium. A predefined intensity thresholding algorithm in ImageJ (NIH) was applied on the Sdf1a-GFP channel to eliminate background. For analysis of the uptake of Sdf1a by the primordium, all values of Sdf1a-GFP outside the ClaudinB mask were discarded. An intensity threshold equal to the average fluorescent intensity of Sdf1a-GFP outside of the primordium in control embryos (*tg(sdf1a:sdf1a-GFP)* embryos stained in the same tube) and a volume threshold of 0.1 μm^3 was applied and the 3D object-counter in ImageJ (NIH), was used to count Sdf1a-GFP puncta within the primordium. A custom ImageJ (NIH) macro language script was written in order to automate this analysis (Data S2). To correct for differences in staining between embryos stained in different tubes, a scaling factor was determined using the average fluorescent intensity of Sdf1a-GFP outside of the primordium in *tg(sdf1a:sdf1a-GFP)* control embryos and applied to all the embryos stained in a given tube. For averaging across embryos of the same genotype, the front of the primordium in each Z-stack was assigned to the 0 μm position, and the number and intensity of Sdf1a-GFP puncta within 150 μm from the front of the primordium were plotted (Figure 2E). For analyzing the distribution of Sdf1a-GFP on the stripe, the ClaudinB mask was inverted and applied to the background-corrected Sdf1a-GFP Z-stack, and Sdf1a-GFP intensities outside the mask were averaged (Data S2). Sdf1a-GFP intensities in embryos of different genotypes were binned and normalized to the average Sdf1a-GFP intensities of wild-type embryos stained in the same tube. For embryos expressing *cxcr7b* from the heat-shock-inducible promoter, Sdf1a-GFP intensities were normalized to the average Sdf1a-GFP intensities in heat-shocked, nontransgenic, wild-type siblings stained in the same tube. For computing the percentage of Sdf1a-GFP that is taken up by wild-type primordia, the Sdf1a-GFP intensity inside the primordia was summed up and divided by the intensity of total Sdf1a-GFP inside and outside the primordium. This analysis was performed over a distance of 150 μm from the tip of the primordium.

Live Imaging Sdf1-Signaling Sensor Embryos

Live *tg(cxcr4b:cxcr4b-Kate2-IRES-EGFP-CaaX)* embryos were mounted in 0.5% low-melt agarose/Ringer's solution (HEPES 5 mM, NaCl 111 mM, KCl 5 mM, CaCl2 1 mM, MgSO4 0.6 mM). Z-stacks were collected with a Leica 40x water dipping lens (NA 0.8) and a Leica SP5 II confocal microscope equipped with HyD detectors (Leica Microsystems) and a heated stage (Warner Instruments). The temperature of the water bath was monitored and maintained between 27.9°C and 28.4°C. All Z-stacks were collected in the photon-counting mode with identical microscope settings with the exception of the time-lapse images, which were collected using multi-point acquisition in order to image multiple embryos over the same imaging period and lower laser powers and a larger pinhole and z-step size in order to collect sufficient light while minimizing bleaching and phototoxicity. For imaging live embryos overexpressing Sdf1a, *tg(hsp70:sdf1a)* embryos were raised at 28°C to 32 hpf. At this time the embryos were heat shocked for 50 min at 37°C, raised at 28°C to 36 hpf, mounted and imaged at 28°C. For imaging live embryos overexpressing Cxcr7b, *tg(hsp70:cxcr7b)* embryos were raised at 28°C to 31 hpf. At this time the embryos were heat shocked for 1 hr at 37°C, raised at 28°C to 36 hpf, mounted and imaged at 28°C. For imaging *cxcr7*-deficient embryos, only primordia that did not migrate further than somite 2 by 36 hpf were imaged. Embryos were genotyped by in situ hybridization and/or PCR as described above.

Quantification of the Sdf1-Signaling Sensor

For the calculation of FmemRed/FmemGreen, a mask was applied to the GFP channel using ImageJ (NIH) with a threshold to selectively mark the cell membranes of the cells that comprise the primordium. All values in the GFP and Kate2 channels outside of the mask were discarded and the photon counts from the Kate2 channel were divided by the photon counts from the GFP channel for each voxel to yield a Z-stack in which each value-containing voxel represents the ratio of Kate2 fluorescence to GFP fluorescence on the cell membrane. For the calculation of FmemGreen, the same procedure was applied as for the calculation of FmemRed/FmemGreen, but only the values in the GFP fluorescence channel were analyzed. For the calculation of FinternalRed/FmemGreen, two masks were applied to the GFP channel with a threshold to selectively mark the cell membranes of the cells that comprise the primordium and with a threshold to mark the entire primordium. The membrane mask was inverted and multiplied with the primordium mask to generate a mask that marks the primordium without its membranes. All values in the Kate2 channel outside of the mask of primordium without its membranes were discarded and the photon counts from the Kate2 channel were divided by the photon counts generated from the FmemGreen calculation. A custom ImageJ (NIH) macro language script was written in order to automate these analyses (Data S3, S4, and S5). The data were then averaged across the dorsal-ventral axis and placed in 1-micron bins in order to yield 100 data points for still images or 80 data points for time-lapse images that correspond to the first 100 μm or the first 80 μm, respectively, from the front of the primordium. A shorter length was used for time-lapse images because the primordium frequently

rounds up and becomes shorter than 100 μm while recovering from a global pulse of Sdf1a. For averaging across embryos with identical genotype, the front of the primordium in each Z-stack was assigned to the 0 μm position. Note: differences in overall ratios in the time-lapse experiments (e.g., Figure 6) compared to the single time-point experiments (e.g., Figure 3 and Figure 4) are due to the different laser power settings that were used for each type of experiment as described in a previous section.

Linearity of the Sdf1-Signaling Sensor

Tg(cxcr4b:cxcr4b-Kate2-IRES-EGFP-CaaX) embryos were injected alternately with 0, 0.5, 1.0 and 1.5 nl of 0.025 mM or 0.1 mM *sdf1a* morpholino solution (Doitsidou et al., 2002). Alternating the injection volumes controls for possible variations in the injection rig and needle over the course of the injection. Uninjected and morphant embryos were imaged alternately at 36 hpf to control for possible variations in the microscope and embryos over the course of imaging. Image collection and gradient quantification were performed as described above. The shift of the Sdf1-signaling gradient was determined by fitting the average ratios to a second order polynomial using the least-squares regression in ImageJ (NIH) and extracting the y-intercept.

Time-Lapse Imaging and Analysis

For time-lapse imaging, embryos were mounted in agarose as described in a previous section. Z-stacks were collected on a Leica SP5 II confocal microscope using a 40x water-dipping objective (NA 0.8) and multi-point acquisition to image multiple wild-type and transgenic embryos simultaneously. For Movies S1 and S4 embryos were imaged every 5 min. For Movie S3, embryos were heat shocked for 20 min at 39°C, rested for 1 hr and imaged every ~5 min starting at 36 hpf. For Movie S5, embryos were heat shocked for 1 hr at 37°C, rested for 2 hr at 28°C and imaged at 5 min intervals for 205 min. For Figure 6, Movie S6 and Figure S7, embryos were heat shocked until the temperature of the embryo medium reached 37°C (10 to 15 min), at which point the embryos were returned to 28°C for a short recovery period and then mounted. Starting several hours later, the embryos were imaged every 10 min over the following 7-8 hr. Figure 6 and Movie S6 represent one trial of this experiment in which eight wild-type and two *cxcr7b*−/− embryos, all carrying *tg(hsp70:sdf1a)*, were imaged simultaneously. Figure S7 represents another trial of this experiment in which four wild-type and four *cxcr7b*−/− embryos, all carrying *tg(hsp70:sdf1a)*, were imaged simultaneously. Movie S7 depicts both trials back-to-back for both genotypes. For videos containing Cxcr4b-Kate2 and memGFP fluorescence composite images, a single Z-slice was isolated and corrected for bleaching by normalizing the images of a stack to the same mean intensity using ImageJ (NIH) (bleach correction macro written by Jens Rietdorf, EMBL, Germany, http://www.embl.de/eamnet/html/downloads.html) (Movie S3, top). For videos showing the FmemRed/FmemGreen ratio fold change (Movie S3, bottom), a single slice from a Z-stack was selected, the ratio of Cxcr4b-Kate2 to memGFP fluorescence was extracted as described above and each frame was normalized to the mean ratio. For videos containing CldnB:lyn$_2$GFP fluorescence images, Z-stacks were converted to maximum intensity projection images using ImageJ (NIH) (Movies S1, S4 and S5). For determining the speed of the primordium in the *tg(hsp70:sdf1a)* embryos described in Figure 6, a maximum intensity projection of the memGFP channel was used to generate a segmented line that tracks the front tip of the primordium through time. A kymograph was then generated based on this line using the MultipleKymograph plugin written for ImageJ by J. Rietdorf and A. Seitz (http://www.embl.de/eamnet/html/body_kymograph.html). Speeds were then attained by running the tsp040421.txt macro (same authors) on a segmented line that tracks the movement of the front tip of the primordium throughout the kymograph. The average speed of 8 primordia was then calculated for each time point.

Calculation of the Slope of the Sdf1-Signaling Gradient

The average FmemRed/FmemGreen ratios across primordia of a given genotype were calculated as discussed above and plotted against the anterior-posterior position in 1-micron bins. To determine the slope of the Sdf1-signaling gradient, the average ratios across the front 100 μm of the primordium were fitted to a linear equation using the least square regression analysis in ImageJ (NIH). For analysis of the recovery of the slope of the Sdf1-signaling gradient in Figure 6, the same approach was used but the mean FmemRed/FmemGreen of the first 80 μm from the tip of the primordium was fitted using linear least square regression. Regression analysis was performed using Prism 6 (GraphPad).

Quantification of the Primordium Migration Defect in Different Genetic Scenarios

Wild-type, *sdf1a*−/− and *cxcr4b*−/− embryos were fixed in 4% paraformaldehyde (Sigma) at 48 hpf and stained for *trop2* mRNA in order to visualize the primordium and determine its position relative to the somites at this stage. For determining the migration defect in the absence of *cxcr7*, *tg(cldnB:lyn$_2$GFP)* embryos in the wild-type and *cxcr7b*−/− genetic backgrounds were injected with the *cxcr7a* morpholino mix and imaged at 48 hpf to determine the position of the primordium relative to the somites. *Tg(cldnB:lyn$_2$GFP); cxcr7b*−/−*; tg(tubb2b:cxcr7b-IRES-CFP-CaaX)* embryos were injected with the *cxcr7a* morpholino mix and imaged at 48 hpf using a Leica 165M FC Fluorescent Stereo Microscope equipped with a Leica DFC345 FX camera.

Calculation of the Fraction of Sdf1a that Participates in Signaling

To calculate the fraction of total Sdf1a that is free to signal, we assumed that the Sdf1-signaling sensor ratios in *cxcr7* deficient embryos report baseline levels of signaling Sdf1a on the stripe and that the Sdf1-signaling sensor ratios in *sdf1a*−/− embryos report the absence of Sdf1a protein. Therefore, the difference in the ratios between these two scenarios corresponds to the total levels of Sdf1a

protein on the stripe ($C_{Sdf1a}(t = 0)$) in terms of Sdf1-signaling sensor ratios (($ratio_{cxcr7} - ratio_{sdf1a}$) = 1.998). The reduction in Sdf1a protein levels is thus given as (($ratio_{sdf1a}$ - $ratio_x$)/1.998) x $C_{Sdf1a}(t = 0)$.

Mosaic Analysis of Cxcr7 Function in Live Embryos

Wild-type *tg (cxcr4b:cxcr4b-Kate2-IRES-EGFP-CaaX)* or *tg (cxcr4b:cxcr4b-Kate2-IRES-EGFP-CaaX)*; *cxcr7b*−/− donor embryos injected with 0.5 to 0.7 nl of *cxcr7a* MO-A (0.5 mM) and *cxcr7a* MO-B (0.5 mM) were injected with Cascade Blue Dextran (Invitrogen) as a lineage tracer at the one cell stage. At the 1000-cell to sphere stage, about 100 *cxcr7* deficient donor cells were transplanted into stage-matched, wild-type *tg (cxcr4b:cxcr4b-Kate2-IRES-EGFP-CaaX)* recipient embryos. Sdf1-signaling across mosaic primordia in live embryos was analyzed as described above, divided into signaling within the clone and the host by applying a mask to the Cascade Blue-labeled donor cells, averaged across the dorsal-ventral and medial-lateral axes and plotted along the anterior-posterior axis using ImageJ (NIH). For the analysis of wild-type cells transplanted into *cxcr7b* mutant embryos, one-cell stage wild-type or *cxcr7b* mutant donor embryos were injected with lysine-fixable biotin-dextran (Invitrogen). At the 1000-cell to sphere stage, ~100 donor cells were transplanted into stage-matched, wild-type or *cxcr7b* mutant recipient embryos. At 36 hpf, primordia were identified by antibody staining using rabbit anti-Kate2 (1:1000, Evrogen) and chicken anti-GFP (1:1000, Abcam) primary antibodies followed by anti- rabbit-Cy3 (1:500, Jackson ImmunoResearch) and anti-chicken-Alexa488 (1:500, Invitrogen) secondary antibodies. The biotin-dextran lineage tracer was detected with streptavidin-Alexa405 (1:1000, Invitrogen). The volume of transplanted cells in the primordium was calculated based on the lineage tracer fluorescence using ImageJ.

Morpholino Injections and Validation

Morpholino sequences (all from Gene Tools):

sdf1a-MO (Doitsidou et al., 2002): 5′-ATCACTTTGAGATCC**ATG**TTTGCA-3′

cxcr7a-MO-A: 5′-AATCCAGGGTTTCGTTCTC**ATG**CGC-3′

cxcr7a-MO-B: 5′-AGCTGAAGTGATCCTGTCTGCGCTT-3′

For assessment of the linearity of the Sdf1-signaling sensor, the *sdf1a* translation-blocking morpholino was used at the following volumes and concentrations: 0, 0.5, 1.0 and 1.5 nL and 0.025 mM and 0.100 mM.

For all experiments involving *cxcr7a* knockdown, *cxcr7a*-MO-A and *cxcr7a*-MO-B were coinjected at the one-cell-stage at a concentration of 0.5 mM each and a volume of 1 nL. In order to verify specific reduction of *cxcr7a* mRNA translation, one-cell-stage embryos were injected with 1 nL of 50 ng/μL *lyn$_2$mCherry* mRNA and 100 ng/μL *cxcr7a-SuperFolderGFP* mRNA alone or 1 nL of 50 ng/μL *lyn$_2$mCherry* mRNA and 100 ng/μL *cxcr7a-SuperFolderGFP* mRNA in addition to 1 nL of *cxcr7a*-Mo-A and 0.5 mM of *cxcr7a*-Mo-B at 0.5 mM each. Embryos were mounted in 0.5% low-melt agarose/Ringer's solution (HEPES 5 mM, NaCl 111 mM, KCl 5 mM, CaCl2 1 mM, MgSO4 0.6 mM) and imaged at ~7 hpf. Z-stacks were collected with a Leica 40x water dipping lens (NA 0.8) and a Leica SP5 II confocal microscope equipped with HyD detectors (Leica Microsystems).

The *cxcr7a-sfGFP* construct was generated by fusing the *cxcr7a* 5′-UTR and coding sequence (excluding the stop codon) to the *Superfolder GFP* coding sequence, separated by a two amino acid GlySer-linker. This construct was subcloned into the pCS2+ expression vector for in vitro mRNA synthesis using the mMessage mMachine kit (Ambion). The following primers were used for cloning:

cxcr7a-sense: ccggagatctAGGATCACTTCAGCTCATCTGCGCATGAGAACGAAACCC

cxcr7a-sfGFP-antisense: CCTTGCTCACCATgctaccAGTCACAGTCGGAGGGTTGTTC

cxcr7a-sfGFP-sense: CCCTCCGACTGTGACTggtagcATGGTGAGCAAGGGCGAGG

sfGFP-antisense: ccggctcgagCTACTTGTACAGCTCGTCCATGC

Global and Local Misexpression of Sdf1a

For ectopic expression of Sdf1a in clones of cells near the primordium, ~50 cells from a 1000-cell to sphere stage *tg(hsp70:sdf1a)* donor embryo were transplanted into a stage-matched *tg(cldnbB:lyn$_2$GFP)* embryo. Embryos were raised at 28°C until 24 hpf. Starting at this stage, embryos were heat shocked at 39°C for 30 min every 3 hr until fixation at approximately 36 hpf. Sdf1a misexpressing cells were identified in fixed embryos by in situ hybridization against *sdf1a* mRNA, and the primordium was identified by antibody staining of GFP protein. For global expression of Sdf1a, *tg(hsp70:sdf1a)* fish were crossed to *tg(cldnbB:lyn$_2$GFP)* fish to obtain double transgenic embryos. These embryos were raised at 28°C until 30 hpf. They were then heat shocked at 39°C from 30 to 31 hpf and from 32 to 32.5 hpf. The embryos were fixed at 32.5 hpf and stained as described above. Brightfield images were collected with on an Axioplan microscope (Zeiss) with a 10x (NA 0.5) or 40x (NA 1.3) oil-immersion objective equipped with an AxioCam camera (Zeiss).

Whole-Mount In Situ Hybridization and Antibody Staining

RNA probe synthesis and in situ hybridization was performed as previously described (Thisse and Thisse, 2008). RNA probes against *kate2*, *trop2*, *cxcr4b*, *sdf1a, cxcr7a and cxcr7b* were labeled with DIG (Roche) and detected with anti-DIG antibody coupled to alkaline phosphatase (1:5000, Roche) and NBT/BCIP (Roche) or anti-DIG coupled to horseradish peroxidase (1:1000, Roche) and Cy3-tyramide signal amplification (Perkin Elmer). For antibody stainings, antibodies against GFP (rabbit anti-GFP, 1:500 Torrey Pines; chicken anti-GFP, Abcam, 1:1000; goat anti-GFP, 1:100, Covance), Kate2 (1:2000, Evrogen) and ClaudinB (1:2000) (Kollmar et al., 2001) were detected with anti-rabbit-Alexa488 (1:500, Invitrogen), anti-rabbit-Cy3 (1:500, Jackson ImmunoResearch),

anti-chicken-Alexa488 (1:500, Invitrogen), anti-goat-Cy3 (1:500, Jackson ImmunoResearch), anti-rabbit-Alexa647 (1:500, Jackson ImmunoResearch) or anti-rabbit-HRP antibody (1:2500, Jackson ImmunoResearch) with DAB (Roche).

SDF1-Signaling Sensor Constructs for Expression in HEK293T Cells

Human *CXCR4* was cloned by including the sequence of exon 1 of *CXCR4* in the forward PCR primer and amplifying exon 2 from genomic DNA obtained from a buccal swab. The receptor was fused to *Kate2-IRES-EGFP-Caax* using assembly PCR to yield *CXCR4-Kate2-IRES-EGFP-Caax*. The construct was cloned into pcDNA3.1+ and verified by sequencing. The fish Sdf1-signaling sensor *cxcr4b-Kate2-IRES-EGFP-Caax* was amplified from the Sdf1-signaling sensor BAC and subcloned into pcDNA3.1+. WHIM mutant versions of the CXCR4 and Cxcr4b receptors were generated using assembly PCR to delete from the SDF1-signaling sensors the sequences coding for amino acids 333-352 of CXCR4 and amino acids 335-353 of Cxcr4b, respectively, and cloned into pcDNA3.1+.

Expression of the SDF1-Signaling Sensor in HEK293T Cells

HEK293T cells were maintained in DMEM supplemented with 10% Bovine Calf Serum, 2mM L-glutamine, 100 units/mL penicillin, and 100 μg/mL streptomycin. For imaging experiments, approximately 3-6x10^5 cells were seeded on 35 mm tissue culture plates and transfected 24 hr after seeding by adding 5 μl Lipofectamine 2000 complexed with 100 ng plasmid DNA in 250 μl Optimem to the growth medium. 24 hr after transfection, expression of the signaling sensors were verified by fluorescence microscopy on a Zeiss Apotome inverted fluorescent microscope. Cells were then washed once with 1 ml Dulbecco's phosphate buffered saline (without calcium and magnesium) and serum-starved for 45min to 1hr in DMEM without phenol red buffered with HEPES prior to chemokine challenge and imaging.

Production of Recombinant Zebrafish Sdf1a

The sequence for active Sdf1a (Sdf1a without the leader peptide) was cloned into pGEX4T1, with a Factor Xa cleavage site directly upstream. Cleavage with Factor Xa results in Sdf1a without any tags or additional amino acid residues. *pGEX4T1-Xa-Sdf1a* was transformed into BL21 *E. coli* (NEB), which were then induced with IPTG for 6 hr after the OD_{600} reached 0.4-0.6, pelleted, and lysed via sonication. Recombinant GST-Sdf1a was purified using Sepharose Fast Flow 4 columns, and the GST tag removed via an on-column digest with Factor Xa (NEB). Elution of Sdf1a was verified using SDS-PAGE followed by silver staining with the Pierce Silver Stain Kit.

Assessing the Linearity of the SDF1-Signaling Sensor In Vitro

Cells expressing the human version of the SDF1-signaling sensor were imaged with a 40x water dipping objective (NA 0.8) on the Leica SP5 II equipped with HyD detectors in photon counting mode. They were then progressively challenged with the addition of 16 nM of recombinant SDF1α (Peprotech) and imaged 45 min after each round of chemokine addition in order to assess the dose-response of the signaling sensor in the same cells and therefore control for between-cell variability in SDF1-signaling sensor expression levels. This was repeated for a total of four consecutive rounds of chemokine addition, with cumulative chemokine concentrations of 16 nM, 32 nM, 48 nM, and 64 nM. The FmemRed/FmemGreen was then calculated for each different cumulative chemokine concentration. A similar procedure was employed for the fish version of the Sdf1-signaling sensor using recombinant Sdf1a for cumulative volumes of 2.5 μL, 5 μL, 10 μL, and 20 μL. WHIM mutant versions of the human and fish SDF1-signaling sensors were challenged with 64 nM of SDF1α and 20 μl of Sdf1a, respectively. They were imaged before addition of chemokine and 45 min after the addition of chemokine. For controls the cells were treated with LIF (gift from Matthias Stadtfeld), a member of the IL6 family of cytokines, at a fincal concentration of xU/ml or with 10 μM of AMD3100 (Sigma), an inhibitor of CXCR4.

Assessing the Specificity of SDF1-Induced CXCR4 Internalization In Vitro by Blocking Receptor Internalization with AMD3100

10 μM of AMD3100 (Sigma) was added to cells expressing the human SDF1-signaling sensor for 30 min before the addition of 64 nM of SDF1α. Cells were imaged before the addition of AMD3100, after 30 min in AMD3100, and 45 min after the addition of SDF1α. The FmemRed/FmemGreen was then calculated for each different treatment condition.

Assessing the Specificity of SDF1-Induced CXCR4 Internalization In Vitro by Challenging with LIF, an Unrelated Cytokine

LIF is a member of the IL6 family of cytokines, and should not signal through CXCR4. We use it to demonstrate that the SDF1-signaling sensor cannot be activated by just any cytokine. Cells expressing the human SDF1-signaling sensor were incubated consecutively with 1 unit/μL and 10 units/μL LIF for 45 min each, and imaged before the addition of LIF, 45 min after the addition of 1 unit/μL LIF, and 45 min after the addition of 9 unit/μL LIF to cells already in media containing 1 unit/μL LIF (cumulative 10 unit/μL LIF). The FmemRed/FmemGreen was then calculated for each different LIF concentrations.

Mathematical Modeling of Chemokine Gradient Formation

The model addresses the question of whether it is feasible for a chemokine sink localized to the rear of the primordium to generate a stable concentration gradient for the chemokine that would be sensed by cells ahead of the sink in the primordium. This gradient would form largely by diffusion, move with the primordium and, in effect, 'bootstrap' the primordium into its self-generated gradient.

The present experiments and other data impose several constraints that must be met by a model. The free diffusion coefficient, D_{free}, for the chemokine, Sdf1, has been measured at about 100 $\mu m^2\ s^{-1}$ (Veldkamp et al., 2005), which is consistent with a protein with molecular mass of 8 kDa (Thorne et al., 2004). The present work shows that the normal velocity of the primordium, u_n, is 0.7μm min^{-1} (0.012 $\mu m\ s^{-1}$) and the concentration gradient forms in about 200 min. The gradient is sensed by a region of primordium that is about 100 μm in extent while the sink extends a variable distance in the rear of the primordium depending on position along the chemokine stripe.

An essential aspect of the model is that it must generate a steady-state condition. Two possible models for gradient formation may be hypothesized. In the first, the motion of the sink attached to the primordium into an essentially infinitely long stripe of chemokine is sufficient to produce a steady-state. In the second, the motion is neglected and the stationary sink in the rear of the primordium will continually remove chemokine leading to an ever-changing gradient unless continuous production and degradation are postulated. Based on the Peclet number it is shown that the first model need not be considered and the second model is developed. Extension of the second model to a moving coordinate system confirms that the moving primordium has little effect for expected values of the effective diffusion coefficient D (which may be less than D_{free}) and u, the velocity of the primordium.

Peclet Number

Many problems involve diffusion and advection where typically a source of diffusing material is present in a flowing medium and the resulting pattern of transport of the material is either affected by both processes or dominated by one. The dominance may be quantified by a dimensionless Peclet number, Pe, that compares the ratio of the characteristic times for diffusion and flow ((Deen, 1998), Chapter 9). Assuming that a characteristic length L_c may be defined for the problem, Pe is defined as the ratio of the diffusion time scale $T_D = L_c^2/D$ to the advection time scale $T_A = L_c/u$ where u is the velocity of the flow so $Pe = T_D/T_A = uL_c/D$. If Pe >> 1 then advection dominates whereas if Pe < < 1 then diffusion dominates.

In the present case there is a moving sink and a stationary medium; nevertheless, symmetry arguments suggest a calculation of Pe is applicable to the present problem, and indeed it has appeared before in discussions of morphogenesis (Howard et al., 2011). Assuming that a characteristic length for the present problem is L_c = 100 μm then, using the above values for D_{free} and u_n, Pe = 0.012, indicating that the motion is not likely to be important. As discussed in the main text, the effective diffusion coefficient, D, may be as low as $D_{free}/20$, however Pe will still be small and diffusion dominant.

Stationary Model with Localized Sink and Distributed Source

The geometry of the model is shown in Figure 7A. A narrow channel of diffusible chemokine with depth in y axis of L (μm) sits above a layer of cells that produce the chemokine so that there is a constant flux J_1 (mol $\mu m^{-2}\ s^{-1}$) into the channel at the lower boundary, $y = 0$. The channel extends indefinitely to the right along the x axis and is terminated on the left at $x = 0$ by an impermeable wall. This is equivalent to the whole system as being reflected at $x = 0$ with no wall. The top of the channel ($y = L$) is also reflecting (no flux) except for the interval $[0 < x < b, y = L]$ where the rear of the primordium forms a sink that absorbs chemokine with flux J_0 (mol $\mu m^{-2}\ s^{-1}$) while the region $[b < x < a, y = L]$ constitutes the front of the primordium where the chemokine gradient is sensed. Far from the sink ($x \geq a$) there must be a constant concentration C_0 (mol μm^{-3}) in the channel and this requires that the chemokine is degraded or otherwise cleared by a constant process that will be characterized here by a first-order rate constant k (s^{-1}). The z-axis is infinitely extended in both directions; because there is no flux in this axis, the width of the channel can be arbitrarily small and impermeable boundaries may be placed at any location.

The governing diffusion equation is

$$\frac{\partial C}{\partial t} = D\left\{\frac{\partial^2 C}{\partial x^2} + \frac{\partial^2 C}{\partial y^2}\right\} - kC \tag{S1}$$

A full solution in this geometry is possible but tedious because the concentration will be distorted near the point (b, L). A detailed solution is not required, however, because the depth in the y axis is small and averaging C in this axis suffices ((Deen, 1998), Chapter 9). The average is given by:

$$\overline{C}(x) = \frac{1}{L}\int_0^L C(x,y)dy.$$

Averaging Eq (S1) in this axis leads to

$$\frac{\partial \overline{C}}{\partial t} = D\left\{\frac{d^2\overline{C}}{dx^2} + \frac{1}{L}\frac{\partial C}{\partial y}\Big|_0^L\right\} - k\overline{C}. \tag{S2}$$

It is convenient to divide problem into two zones, with new space variables x_1, x_2, and use the standard definition of flux together with the boundary conditions described above, so that in

$$\text{Zone A}: 0<x_1<b: J_0 = -D\frac{\partial C}{\partial y}\Big|^{L} \text{ and } J_1 = -D\frac{\partial C}{\partial y}\Big|_{0} \text{ and in}$$

$$\text{Zone B}: b<x_2<\infty: 0 = -D\frac{\partial C}{\partial y}\Big|^{L} \text{ and again, } J_1 = -D\frac{\partial C}{\partial y}\Big|_{0}.$$

Inserting these boundary conditions in Eq (S2) and defining new variables C_1 and C_2 for the y-averaged concentrations in the two zones yields

$$\frac{\partial C_1}{\partial t} = D\frac{\partial^2 C_1}{\partial x_1^2} - \frac{J_0}{L} + \frac{J_1}{L} - kC_1, \tag{S3a}$$

$$\frac{\partial C_2}{\partial t} = D\frac{\partial^2 C_2}{\partial x_2^2} + \frac{J_1}{L} - kC_2. \tag{S3b}$$

The equations now involve only independent variables (x, t) so at the ends of the channel the following boundary conditions apply: $J_{x1}(0, t) = 0$, $J_{x2}(\infty, t) = 0$. At the boundary between zones: $J_{x1}(b, t) = J_{x2}(b, t)$ and $C_1(b, t) = C_2(b, t)$.

This problem may be solved using the Laplace transform method where

$$C^*(x,s) = \int_0^\infty \exp(-st)C(x,t)dt.$$

Then Eqs (S3a, b) become:

$$\frac{D}{k+s}\frac{d^2C_1^*}{dx_1^2} - \frac{J_0 - J_1}{Ls(k+s)} - C_1^* = 0 \tag{S4a}$$

$$\frac{D}{k+s}\frac{d^2C_2^*}{dx_2^2} + \frac{J_1}{Ls(k+s)} - C_2^* = 0 \tag{S4b}$$

where starred variables ('*') denote the Laplace transforms of the concentrations and it is assumed that $C_1(x_1, 0+) = C_2(x_2, 0+) = C_0$ (see below for evaluation of C_0).

Eqs (S4a, b) are ordinary differential equations in either x_1 or x_2 and have standard solutions as the sum of exponentials with arguments $\pm\sqrt{(k+s)x/D}$. Solving and applying boundary conditions defined above (after taking the Laplace transform where appropriate) and assuming that the source J_1 is on at all times while the sink J_0 commences at $t = 0$, then performing the requisite algebra, yields solutions in Laplace space:

$$C_1^*(x_1,s) = \frac{1}{sL}\left[\frac{J_1}{k} - \frac{J_0}{k+s}\left(1 - \exp\left(-\sqrt{\frac{k+s}{D}}b\right)\cosh\left(\sqrt{\frac{k+s}{D}}x_1\right)\right)\right] \tag{S5a}$$

$$C_2^*(x_2,s) = \frac{1}{sL}\left[\frac{J_1}{k} - \frac{J_0}{k+s}\sinh\left(\sqrt{\frac{k+s}{D}}b\right)\exp\left(\sqrt{\frac{k+s}{D}}x_2\right)\right]. \tag{S5b}$$

By expanding the hyperbolic functions as exponentials and applying a succession of standard Laplace transform relations (Doetsch, 1971), the inverse Laplace transforms may be obtained:

$$C_1(x_1,t) = \frac{J_1}{kL} - \frac{J_0}{kL}(1 - \exp(-kt)) + \frac{J_0}{2L}\int_0^t \left[\operatorname{erfc}\left(\frac{b - x_1}{2\sqrt{D\xi}}\right) + \operatorname{erfc}\left(\frac{b + x_1}{2\sqrt{D\xi}}\right)\right]\exp(-k\xi)d\xi, \tag{S6a}$$

$$C_2(x_2,t) = \frac{J_1}{kL} - \frac{J_0}{2L}\int_0^t \left[\operatorname{erfc}\left(\frac{x_2 - b}{2\sqrt{D\xi}}\right) - \operatorname{erfc}\left(\frac{x_2 + b}{2\sqrt{D\xi}}\right)\right]\exp(-k\xi)d\xi. \tag{S6b}$$

It is clear that at $t = 0$,

$C_1(x_1,0)=C_2(x_2,0)=C_0=J_1/kL$, which is the steady concentration in the channel above the stripe representing a balance between the distributed source J_1 and the degradation process characterized by the rate constant k. Therefore, Eqs (S6a, b) may be normalized by dividing through by C_0 to obtain

$$\frac{C_1}{C_0}=1-R(1-\exp(-kt))+\frac{Rk}{2}\int_0^t\left[\operatorname{erfc}\left(\frac{b-x_1}{2\sqrt{D\xi}}\right)+\operatorname{erfc}\left(\frac{b-x_1}{2\sqrt{D\xi}}\right)\right]\exp(-k\xi)d\xi \tag{S7a}$$

$$\frac{C_2}{C_0}=1-\frac{Rk}{2}\int_0^t\left[\operatorname{erfc}\left(\frac{x_2-b}{2\sqrt{D\xi}}\right)-\operatorname{erfc}\left(\frac{x_2+b}{2\sqrt{D\xi}}\right)\right]\exp(-k\xi)d\xi \tag{S7b}$$

where $R=J_0/J_1$ is the ratio of the localized sink flux to the distributed source flux.

It is also useful to state the steady-state solutions to the problem i.e., the result as $t\to\infty$. This may be derived immediately from Eqs (S5a, b) by noting that $C(x,\infty)=\lim_{s\to 0} sC^*(x,s)$ (Doetsch, 1971) to obtain

$$\frac{C_1(x_1,\infty)}{C_0}=1-R\left(1-\exp\left(-\sqrt{\frac{k}{D}}b\right)\cosh\left(\sqrt{\frac{k}{D}}x_1\right)\right) \tag{S8a}$$

$$\frac{C_2(x_2,\infty)}{C_0}=1-R\sinh\left(\left(\sqrt{\frac{k}{D}}b\right)\exp\left(-\sqrt{\frac{k}{D}}x_2\right)\right). \tag{S8b}$$

The experimental data indicate that the baseline concentration of chemokine under the sink in the steady-state, C_b, is about 0.14 × C_0. In order to start the gradient from that value in each calculation, Eq (S8a) was used to define R as

$$R\left(\frac{C_b}{C_0}\right)=\frac{(1-C_b/C_0)}{\left(1-\exp\left(-b\sqrt{k/D}\right)\right)}.$$

Moving Coordinates

As noted above, the Peclet number indicates that the motion of the primordium contributes little to the shape of the gradient, which is dominated by diffusion for the values of D and u in this situation. The effect of movement may be incorporated in Eqs (S7a, b) by appropriate analysis, which will not be described in detail here. Suffice to note that in the usual advection or flow problem, the medium moves and a source is either stationary or carried with the flow and a transformation is made to moving coordinates where the diffusion problem is solved. Here the medium is stationary, while the sink moves, and it is desired to see the gradient from the perspective of the moving primordium, where the sink is located. It may be shown that this is accomplished by the following substitutions: $x\to\eta+u\tau;\ \ t\to\tau$ in Eqs (S7a, b) where η and τ are the coordinates in the moving frame. This substitution has been made to calculate some of the results shown in Figure 6H and Figure 7.

Calculations

All equations were evaluated using Matlab 2012b (MathWorks, Natick, MA). The integrals in Eqs (S7a, b) were performed with the built-in function 'integral', which uses global adaptive quadrature, with default tolerances.

Interpretation

In order to make the calculations shown in Figure 6H and Figure 7 it was necessary to choose a value for the rate constant that defines the degradation or clearance process. Our calculations and the literature (Kicheva et al., 2007) suggest that k = 0.0003 s^{-1} is a reasonable value. Based on extensive calculations (not shown) we found that the value of k largely determined how rapidly the chemokine gradient reached a steady-state and that a value of k = 0.0003 s^{-1} was appropriate for the ~200 min time frame observed experimentally.

Figures 7B shows Eqs (S7a, b) evaluated at various times for $D=D_{free}$ = 100 $\mu m^2\ s^{-1}$, the assumed free diffusion coefficient for Sdf1. The solid lines show the solution for u = 0 (Eqs S7a, b); the effect of motion with $u=u_n$ = 0.7 $\mu m\ min^{-1}$ is shown as dashed lines, which are effectively superimposed on the u = 0 lines here, showing that the effect of movement is imperceptible. For the part of curve beyond the sink (which extends from 0 to 20 μm here; a longer sink does not have much effect of the results), the gradient is a straight line indicating that the argument of the exponential in Eq (S7b) is sufficiently small that it may be represented by the linear part of the series expansion. It is seen that by 200 min after activating the sink, the gradient has reached the steady-state curve, shown as a dotted black line (Eqs S8a, b). To show that a sufficiently high primordium velocity can affect the gradients, Figure 7B shows the effect increasing u to 20 × u_n. Now a steady-state is apparently reached by about 120 min and the gradients are steeper

reflecting the fact that the primordium is 'pushing into' the reservoir of chemokine in the stripe. Note, however, that even this non-physiological velocity does not affect the overall shape of the gradient.

Returning to Figure 7A it is apparent that the gradient evolves to a steady-state in the requisite time and is linear, but the slope is smaller than that observed experimentally. Figures 7D and 7E explore the possibility that the reason for the shallow slope is that the assumed value of the diffusion coefficient is inappropriate. In many systems the chemokine or morphogen interacts with the extracellular matrix, most often with the heparin sulfate component, which may result in an effective diffusion coefficient that is considerably smaller than D_{free}. This is also true in other contexts e.g., Thorne et al. (2008). In Figure 7D, the effective diffusion coefficient D is set at $D_{free}/4$ while in Figure 7E it is $D_{free}/20$. It is evident that as D decreases, the slope of the gradient increases and in Figure 7E it is close to the slope observed experimentally (see Figure 6G, H). This suggests that a reduced D is indeed at work here. Looking again at the last panel it is seen that the gradient is now departing from a straight line as the exponential nature of the curve becomes more apparent (actually the whole curve, if extended beyond 100 μm would be sigmoidal as it asymptotically approached unity). It is also apparent that, with a reduced diffusion coefficient, the effect of primordium motion, though still small, begins to become more evident.

Comparison to Crick Model

The model proposed by Crick (1970) for diffusion embryogenesis is widely cited. It envisages a discrete source of morphogen and discrete sink separated by 50-100 cells through which the morphogen travels with an effective diffusion coefficient. The source is represented by a constant concentration boundary condition and the sink is represented by a zero concentration boundary condition. Actually, this type of problem was solved earlier by Carslaw and Jaeger ((Carslaw and Jaeger, 1959), section 3.4) from which the time evolution may be easily derived without ad hoc arguments. By necessity Crick's model arrives at a linear gradient in the steady-state, although the time-evolution of the gradients is quite complex in shape and would not mimic the present experimental results because of Crick's fixed concentration at the sink. In the present situation, the sink might be approximated by a point-sink but the need to have a stable stripe of chemokine over a very long distance excludes a localized source while also necessitating a degradation process. The present model only generates a linear steady-state gradient when the gradient is quite shallow but allowing the primordium to release an additional substance that inhibits chemokine production might generate a steeper, linear gradient.

Regulation of *cxcr4b* Expression by *cxcr7a*

Quantification of GFP expression from the Sdf1-signaling sensor indicates that the expression of *cxcr4b* is reduced by 25% in *cxcr7a* but not *cxcr7b* deficient embryos and that this reduction is dependent on *sdf1a* activity (Figure S2). This suggests that Cxcr7a may have two functions – clearing Sdf1 and promoting *cxcr4b* expression. Consistent with this supposition, studies in other systems have shown that CXCR7 acts both as a signaling receptor and a chemokine clearance receptor (Odemis et al., 2010; Rajagopal et al., 2010; Sánchez-Alcañiz et al., 2011; Wang et al., 2012). However, Cxcr7a's role in promoting *cxcr4b* expression is not essential for primordium migration since the expression of *cxcr7b* in the posterior lateral line axons underneath the rear of the primordium restores primordium migration in *cxcr7* deficient embryos (Figure 1D and S6). This suggests that Cxcr7a's critical function during primordium migration is to remove Sdf1a protein from underneath the rear of the primordium together with Cxcr7b to generate a Sdf1-signaling gradient across the primordium and promote its migration.

SUPPLEMENTAL REFERENCES

Carslaw, H.S., and Jaeger, J.C. (1959). Conduction of Heat in Solids (Oxford, UK: Clarendon Press).

Deen, W. (1998). Analysis of Transport Phenomenon (New York: Oxford University Press).

Doetsch, G. (1971). Guide to the Applications of the Laplace and Z-Transforms (New York: Van Nostrand-Reinhold).

Doitsidou, M., Reichman-Fried, M., Stebler, J., Köprunner, M., Dörries, J., Meyer, D., Esguerra, C.V., Leung, T., and Raz, E. (2002). Guidance of primordial germ cell migration by the chemokine SDF-1. Cell *111*, 647–659.

Howard, J., Grill, S.W., and Bois, J.S. (2011). Turing's next steps: the mechanochemical basis of morphogenesis. Nat. Rev. Mol. Cell Biol. *12*, 392–398.

Kettleborough, R.N.W., Busch-Nentwich, E.M., Harvey, S.A., Dooley, C.M., de Bruijn, E., van Eeden, F., Sealy, I., White, R.J., Herd, C., Nijman, I.J., et al. (2013). A systematic genome-wide analysis of zebrafish protein-coding gene function. Nature *496*, 494–497.

Knaut, H., Werz, C., Geisler, R., and Nüsslein-Volhard, C.; Tübingen 2000 Screen Consortium. (2003). A zebrafish homologue of the chemokine receptor Cxcr4 is a germ-cell guidance receptor. Nature *421*, 279–282.

Knaut, H., Blader, P., Strähle, U., and Schier, A.F. (2005). Assembly of trigeminal sensory ganglia by chemokine signaling. Neuron *47*, 653–666.

Kollmar, R., Nakamura, S.K., Kappler, J.A., and Hudspeth, A.J. (2001). Expression and phylogeny of claudins in vertebrate primordia. Proc. Natl. Acad. Sci. USA *98*, 10196–10201.

Kwan, K.M., Fujimoto, E., Grabher, C., Mangum, B.D., Hardy, M.E., Campbell, D.S., Parant, J.M., Yost, H.J., Kanki, J.P., and Chien, C.-B. (2007). The Tol2kit: a multisite gateway-based construction kit for Tol2 transposon transgenesis constructs. Dev. Dyn. *236*, 3088–3099.

Lewellis, S.W., Nagelberg, D., Subedi, A., Staton, A., LeBlanc, M., Giraldez, A., and Knaut, H. (2013). Precise SDF1-mediated cell guidance is achieved through ligand clearance and microRNA-mediated decay. J. Cell Biol. *200*, 337–355.

Odemis, V., Boosmann, K., Heinen, A., Küry, P., and Engele, J. (2010). CXCR7 is an active component of SDF-1 signalling in astrocytes and Schwann cells. J. Cell Sci. *123*, 1081–1088.

Rajagopal, S., Kim, J., Ahn, S., Craig, S., Lam, C.M., Gerard, N.P., Gerard, C., and Lefkowitz, R.J. (2010). β-arrestin- but not G protein-mediated signaling by the "decoy" receptor CXCR7. Proc. Natl. Acad. Sci. USA *107*, 628–632.

Thorne, R.G., Hrabetová, S., and Nicholson, C. (2004). Diffusion of epidermal growth factor in rat brain extracellular space measured by integrative optical imaging. J. Neurophysiol. *92*, 3471–3481.

Thorne, R.G., Lakkaraju, A., Rodriguez-Boulan, E., and Nicholson, C. (2008). In vivo diffusion of lactoferrin in brain extracellular space is regulated by interactions with heparan sulfate. Proc. Natl. Acad. Sci. USA *105*, 8416–8421.

Wang, Y., Li, G., Stanco, A., Long, J.E., Crawford, D., Potter, G.B., Pleasure, S.J., Behrens, T., and Rubenstein, J.L.R. (2012). CXCR4 and CXCR7 have distinct functions in regulating interneuron migration. Neuron *442*, 433–442.

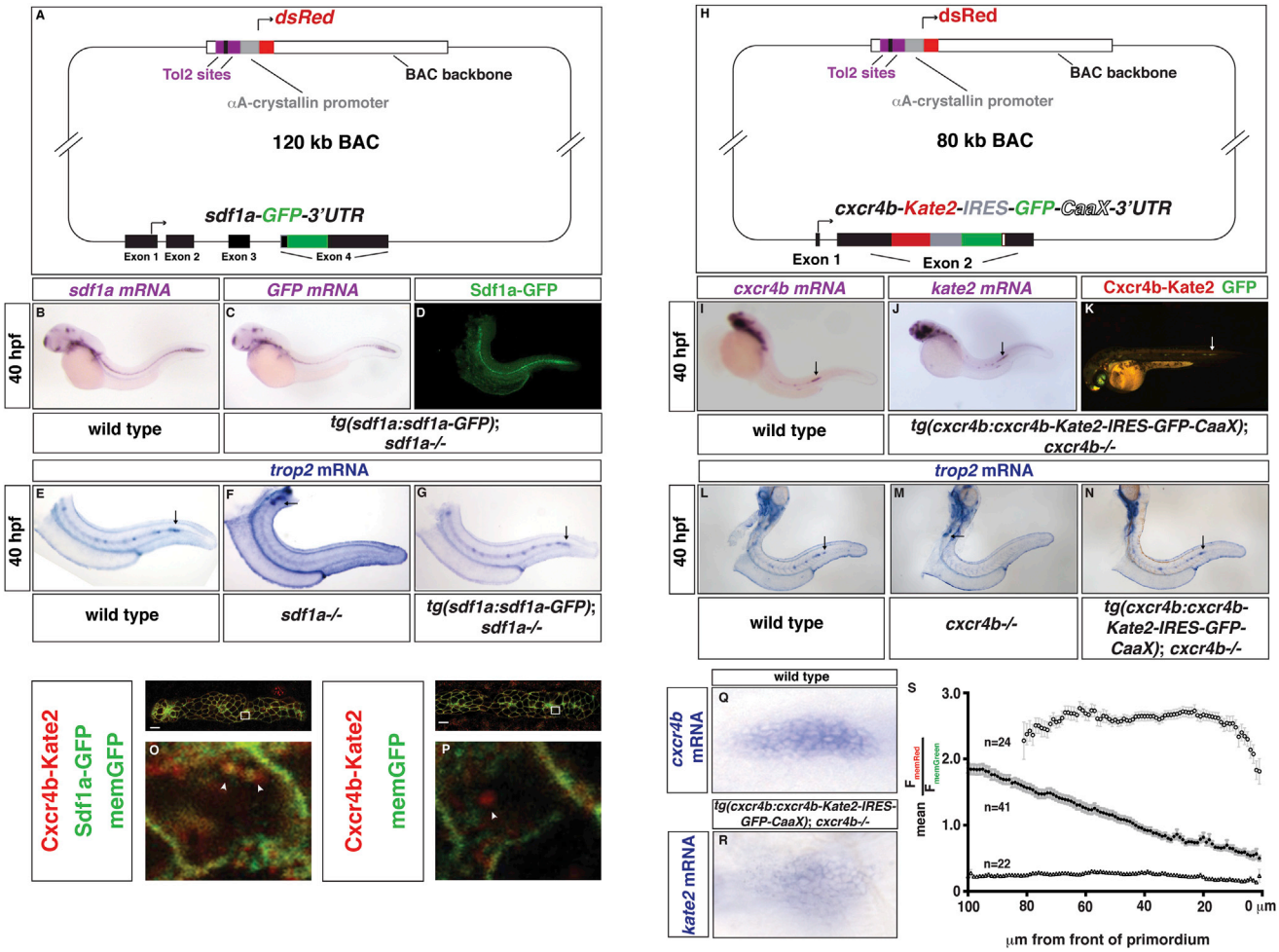

Figure S1. Characterization of the Transgenic Fish Lines *tg(sdf1a:sdf1a-GFP)* and *tg(cxcr4b:cxcr4b-Kate2-IRES-GFP-CaaX)*, Related to Figures 2, 3, and 4

(A) Schematic overview of the *sdf1a:sdf1a-GFP* transgene. (B) 40 hpf wild-type embryo stained for *sdf1a* mRNA. (C, D) 40 hpf *tg(sdf1a:sdf1a-GFP)p10*; *sdf1a*−/− embryos stained for *GFP* mRNA (C) or Sdf1a-GFP protein (D). (E–G) *trop2* mRNA staining labeling the primordium and deposited neuromasts in 40 hpf wild-type (E), *sdf1a*−/− (F) and *tg(sdf1a:sdf1a-GFP)p10*; *sdf1a*−/− embryos (G). (H) Schematic overview of the *cxcr4b:cxcr4b-Kate2-IRES-eGFP-CaaX* transgene. (I–K) (I) 40 hpf wild-type embryo stained for *cxcr4b* mRNA. (J, K) 40 hpf *tg(cxcr4b:cxcr4b-Kate2-IRES-GFP-CaaX)p7*; *cxcr4b*−/− embryos stained for *kate2* mRNA (J) or imaged live for Kate2 and GFP fluorescence (K). Arrows in J to K indicate the primordium. (L–N) *trop2* mRNA staining labeling the primordium and deposited neuromasts in 40 hpf wild-type (L), *cxcr4b*−/− (M) and *tg(cxcr4b:cxcr4b-Kate2-IRES-GFP-CaaX)p7*; *cxcr4b*−/− embryos (N). Arrows in (E–G) and (L–N) indicate the extent of primordium migration. (O and P) Primordium from a 28 hpf *tg(sdf1a:sdf1a-GFP)p10; tg(cxcr4b:cxcr4b-Kate2-IRES-GFP-CaaX); cxcr7b*−/− embryo (O) and primordium from a 28 hpf *tg(cxcr4b:cxcr4b-Kate2-IRES-GFP-CaaX); cxcr7b*−/− embryo (P) stained for Kate2 (red) and GFP (green). (O) and (P) represent cells bounded by the white box in the overview image of the primordium. Arrowheads indicate the colocalization of Sdf1a-GFP and Cxcr4b-Kate2 puncta in O and Cxcr4b-Kate2 in P. (Q–R) High resolution images of the primordium in a 40 hpf wild-type embryo stained for *cxcr4b* mRNA (Q) and 40 hpf *tg(cxcr4b:cxcr4b-Kate2-IRES-GFP-CaaX)p7*; *cxcr4b*−/− embryo stained for *kate2* mRNA (R). (S) Mean FmemRed/FmemGreen ratio values across primordia from wild-type (solid circles), *sdf1a*−/− (triangles) and *tg(hsp70:sdf1a)* embryos (open circles). The front of the primordium is at 0 μm. The gray bars indicate SEM.

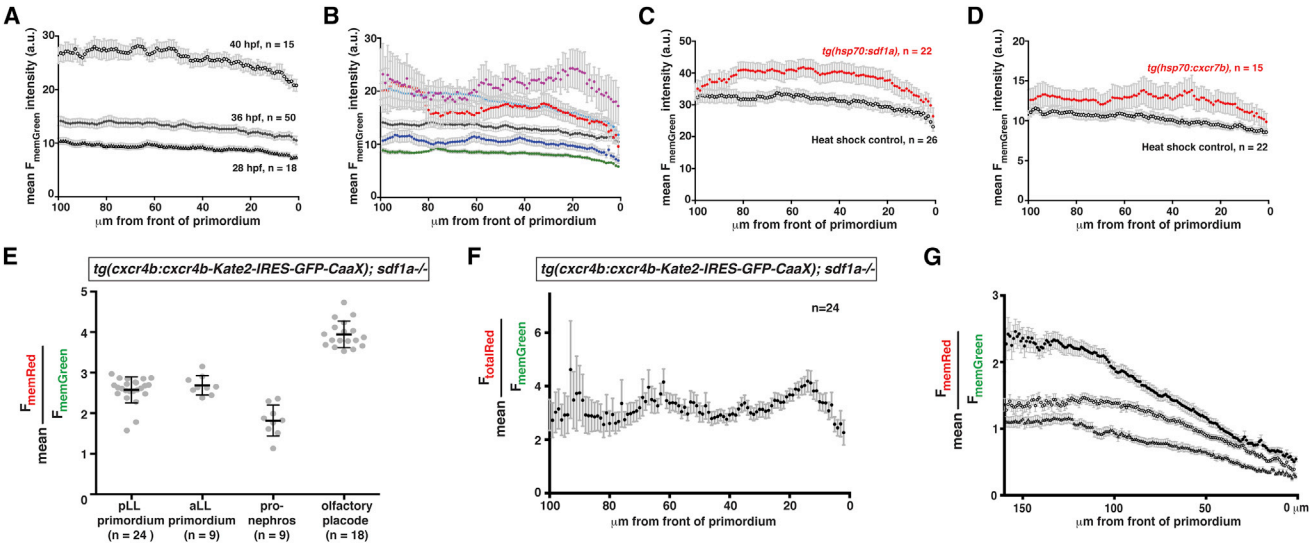

Figure S2. Characterization of the Sdf1-Signaling Sensor, Related to Figures 3 and 4

(A–D) Mean FmemGreen intensity values across 100 μm beginning at the front of the primordium in (A) wild-type embryos at 28, 36 and 40 hpf (triangles, solid circles and open circles, respectively), (B) wild-type (gray, n = 50), *sdf1a* mutant embryos (red, n = 24), *cxcr7a* morphants (green, n = 37), *cxcr7b* mutants (light blue, n = 62), *cxcr7* deficient embryos (dark blue, n = 29) and *sdf1a* and *cxcr7* deficient (magenta, n = 10) embryos, (C) *sdf1a* overexpressing embryos and (D) *cxcr7b* overexpressing embryos at 36 hpf. Note that the heat shock regimen for *sdf1a* overexpressing embryos and *cxcr7b* overexpressing embryos are different (see Extended Experimental Procedures). The front of the primordium is at 0 μm.

(E) Mean FmemRed/FmemGreen across the tissue of the posterior lateral line (pLL), the anterior lateral line (aLL), the pronephros and olfactory neurons. The horizontal black bars indicate the average and the error bars represent SD.

(F) Mean FtotalRed/FmemGreen values across 100 μm beginning at the front of *sdf1a*−/− primordia.

(G) Mean FmemRed/FmemGreen ratio values across 160 μm beginning at the front of the primordium in wild-type (solid circles, n = 34), *cxcr7a* morphant (open circles, n = 27) and *cxcr7b* mutant embryos (open triangles, n = 25). The front of the primordium is at 0 μm. Anterior is to the left for (A–D), (F), and (G) and error bars represent SEM.

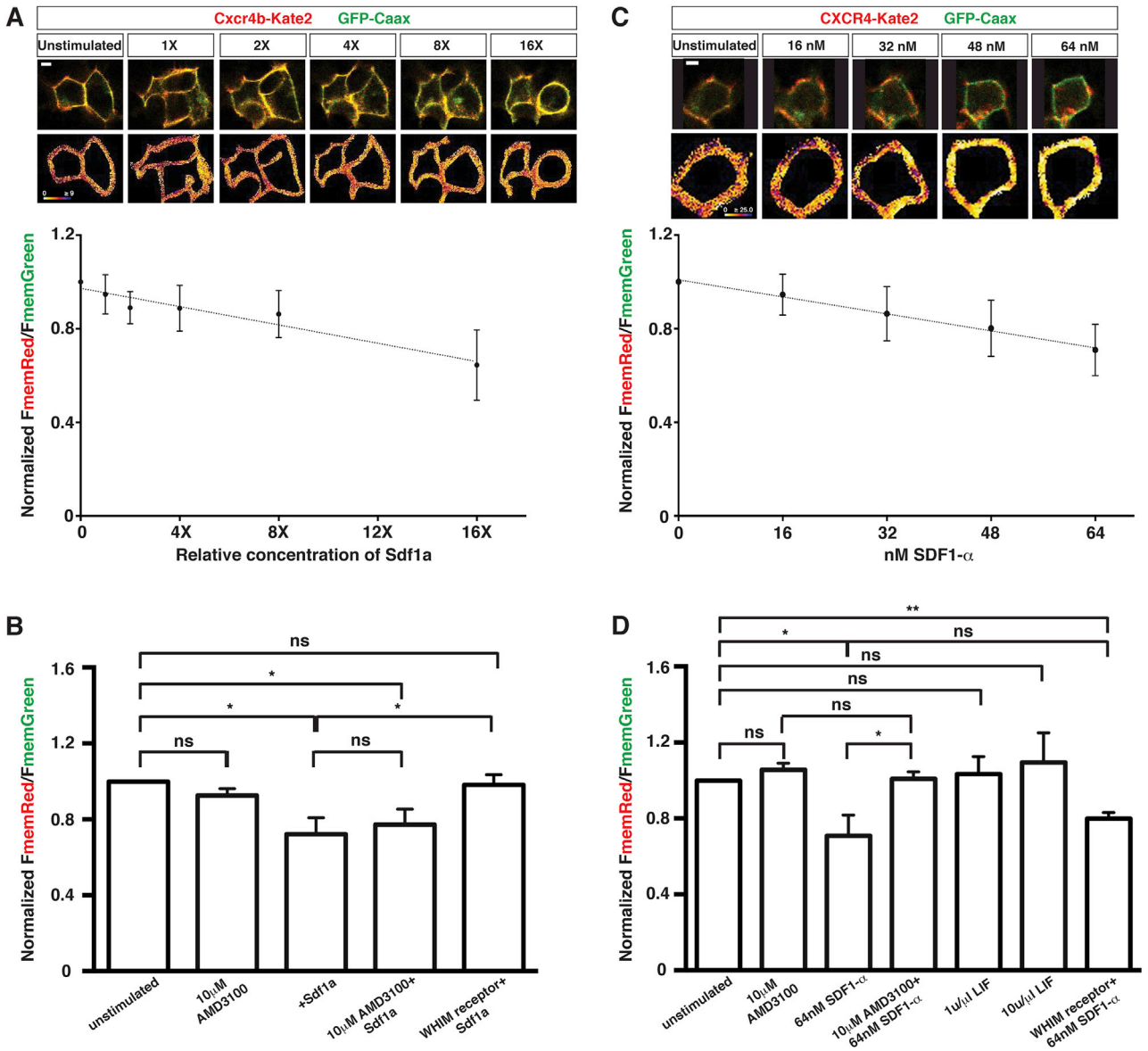

Figure S3. Human and Zebrafish Versions of the Sdf1-Signaling Sensor Respond Linearly and Specifically to Increasing Extracellular Concentrations of Sdf1 Protein In Vitro, Related to Figure 3

(A) Response of fish Sdf1-signaling sensor expressed in HEK293T cells to increasing relative concentrations of purified, recombinant zebrafish Sdf1a (n = 5). The line represents the linear regression of relative concentrations of Sdf1a versus normalized FmemRed/FmemGreen. The R^2 of the regression is 0.9313. FmemRed/FmemGreen ratios are normalized to the membrane ratios of unstimulated cells. Representative composite images of Cxcr4b-Kate2 and GFP at each Sdf1a concentration are shown above the graph.

(B) Response of the Sdf1-signaling sensor to extracellular Sdf1a after blocking receptor internalization with AMD3100 or the WHIM mutation (n = 5). Note that AMD3100 does not appear to antagonize the fish Cxcr4b receptor. FmemRed/FmemGreen ratios are normalized to the membrane ratios of unstimulated cells expressing the same version of the signaling sensor. The same amount of Sdf1a was added for all conditions marked with +Sdf1a.

(C) Response of human SDF1-signaling sensor expressed in HEK293T cells to increasing concentrations of recombinant human SDF1α. The line represents the linear regression of relative concentrations of SDF1α versus normalized FmemRed/FmemGreen. The R^2 of the regression is 0.9312. Representative composite images of CXCR4-Kate2 and GFP at each SDF1α concentration are shown above the graph.

(D) Response of the Sdf1-signaling sensor to extracellular SDF1α after blocking receptor internalization with AMD3100 or the WHIM mutation and upon stimulation with an unrelated recombinant cytokine, LIF. FmemRed/FmemGreen ratios are normalized to the membrane ratios of unstimulated cells expressing the same version of the signaling sensor. Error bars in (A–D) represent SEM. Scale bar represents 5 μχρονσ. * = $p < 0.05$, ** = $p < 0.01$, ns = $p > 0.05$ (not statistically significant).

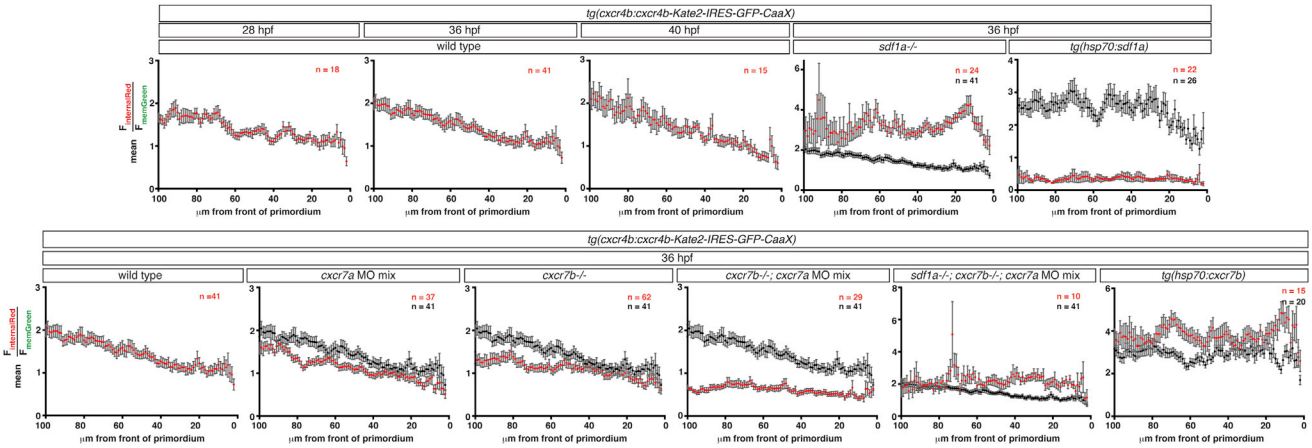

Figure S4. Gradient of Internalized Cxcr4b-Kate across the Primordium, Related to Figures 3 and 4

Mean FinternalRed/FmemGreen ratio values across 100 μm beginning at the front of the primordium in embryos of the indicated genotypes. The front of the primordium is at 0 μm. The gray bars indicate SEM. The black circles where present indicate the mean FinternalRed/FmemGreen of wild-type embryos or heat shocked control embryos represent heat-shocked wild-type control embryos. Note the differences in scale of the Y-axes.

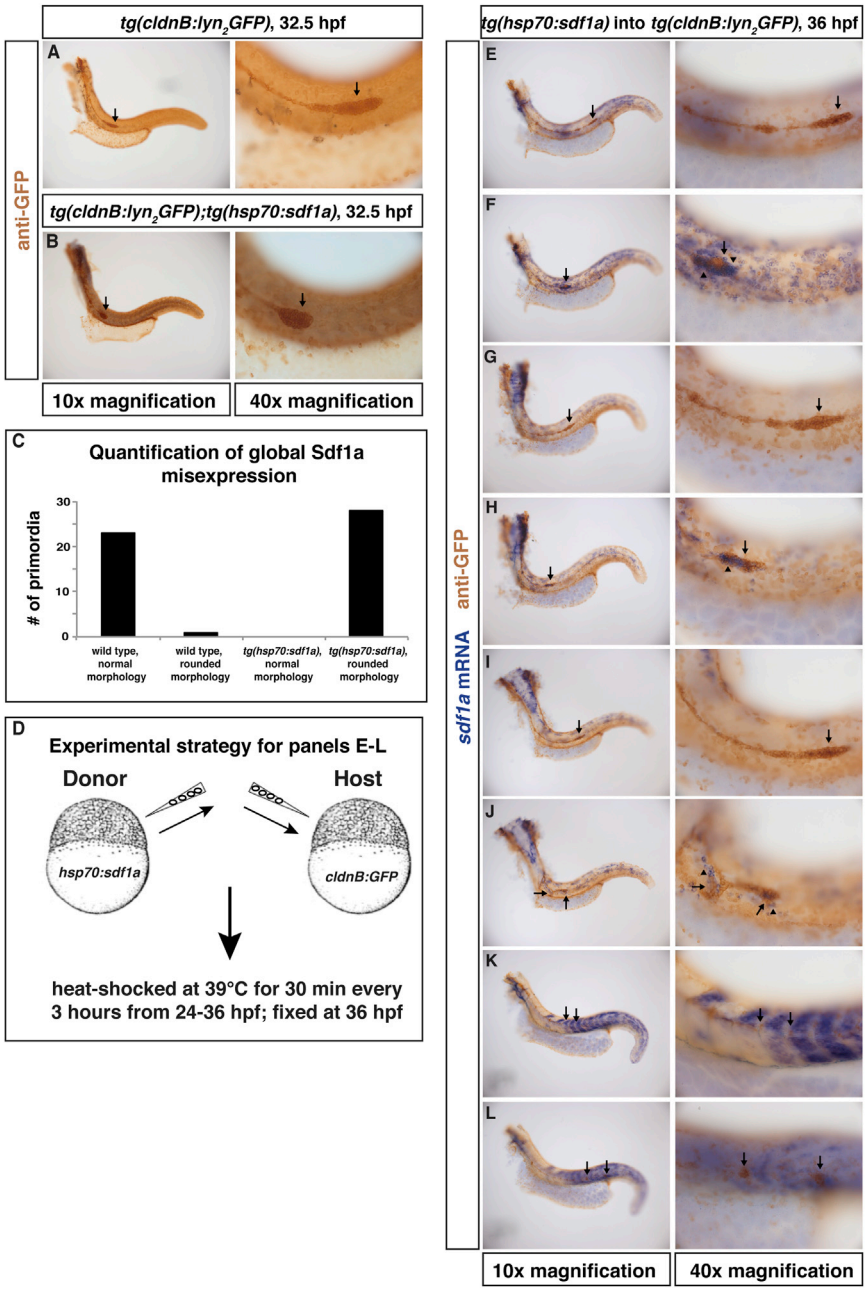

Figure S5. Ectopic Sources of Sdf1a Attract the Primordium, Related to Figure 3

(A) Heat-shocked *tg(cldnB:lyn$_2$GFP)* embryo stained for GFP protein (brown) to visualize the primordium (arrow). (B) Similarly treated *tg(cldnB:lyn$_2$GFP)*; *tg(hsp70:sdf1a)* embryo. (C) Quantification of primordia morphology in heat-shocked wild-type and *tg(hsp70:sdf1a)* embryos. (D) Experimental strategy for local mis-expression of Sdf1a during primordium migration.

(E–L) 36 hpf chimeric embryos comprised of *tg(hsp70:sdf1a)* donor cells and *tg(cldnB:lyn$_2$GFP)* host cells. Embryos were stained for GFP protein to visualize the primordium (arrow) and *sdf1a* mRNA to identify donor cells that overexpress *sdf1a*. (E and F) Sdf1a mis-expression in some of the front and rear cells of the primordium (arrowheads in F) disrupts its migration (arrow in F) compared to the primordium on the contralateral control side of the same embryo (arrow in E). (G and H) Sdf1a mis-expression in the rear cells of the primordium (arrowhead in H) stalls primordium migration (arrow in H) compared to the contralateral control side of the same embryo (arrow in G). (I and J) Sdf1a mis-expression along the migratory route (arrowheads in J) redirects the primordium to the ectopic Sdf1a source (arrows in J) compared to the contralateral control side of the same embryo (I). (K and L) Sdf1a mis-expression in the somites results in a fragmented primordium (arrows in K and L) on both sides of the embryo.

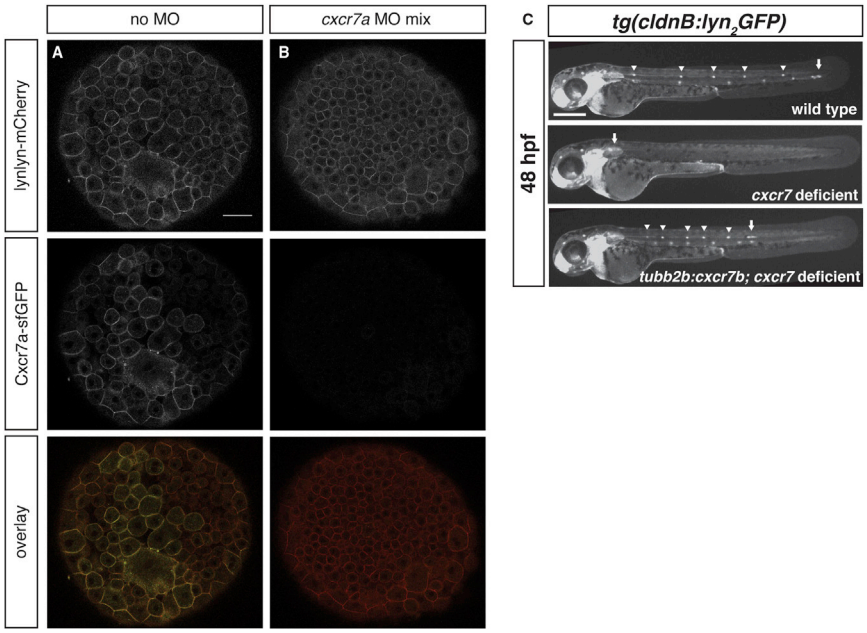

Figure S6. Characterization of *cxcr7a* Morpholino Mix and Rescue of Primordium Migration in *cxcr7*-Deficient Embryos Expressing *cxcr7b* in the Posterior Lateral Line Nerve, Related to Figures 1 and 4

(A and B) Confocal sections through embryos injected with an mRNA mix coding for *cxcr7a-sfGFP* and *lyn$_2$-mCherry* without (A) or with translation blocking *cxcr7a* morpholinos A and B (B). Scale bar, 30 μm.

(C) Position of primordia in representative embryos of the indicated genotypes. Scale bar 300 μm.

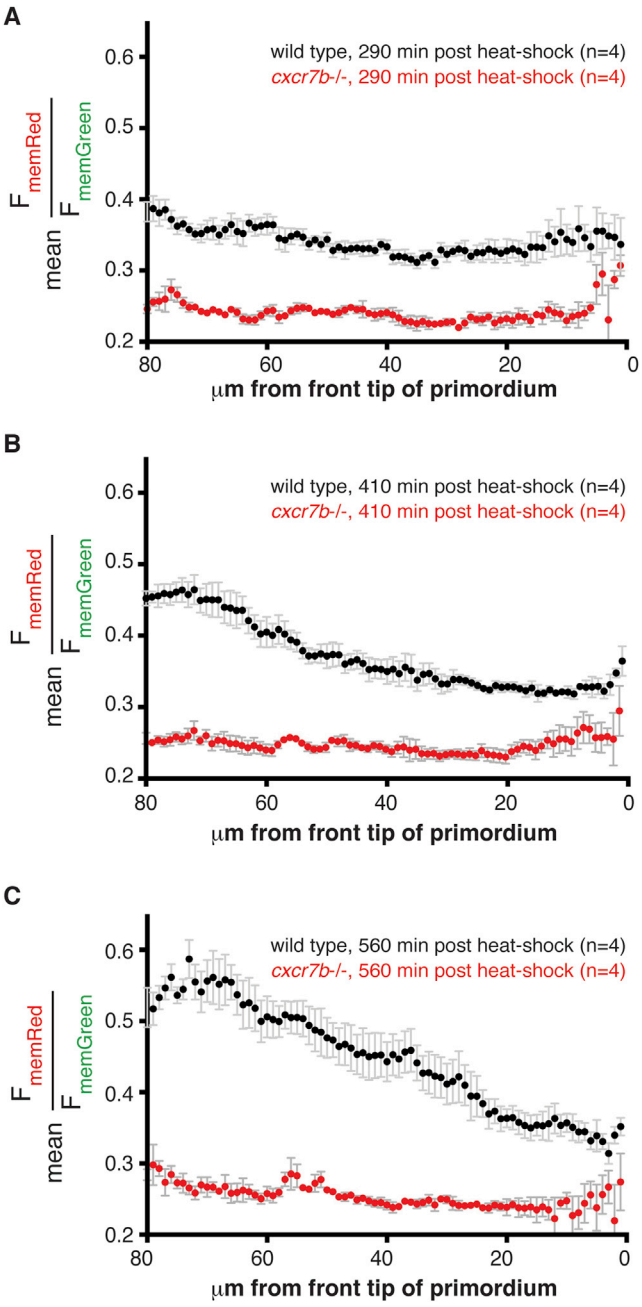

Figure S7. Cxcr7b Activity Is Required for Recovery of the Sdf1-Signaling Gradient, Related to Figure 6

Graphs represent the mean FmemRed/FmemGreen ratio values across the primordium at the indicated times following a pulse of global Sdf1a expression. Black circles represent *tg(hsp70:sdf1a)* embryos; red circles represent *tg(hsp70:sdf1a); cxcr7b−/−* embryos. Grey bars indicate SEM. These data were derived from a second, independent trial of the experiment shown in Figure 6.

(A) Abrogation of the Sdf1-signaling gradient. (B) Initiation of Sdf1-signaling gradient recovery in wild-type but not in *cxcr7b−/−* embryos. (C) Full recovery of the linear Sdf1-signaling gradient in wild-type embryos but not in *cxcr7b−/−* embryos.